THE DETECTION OF SECOND-ORDER COHERENCE EFFECTS IN AN OPTICAL FIELD

Joan Lang McMillan, B.Sc.

Master of Philosophy

University of Edinburgh

1978

CONTENTS

ABSTRACT

An experiment, which was designed to detect and measure the spatial modulation of the degree of second-order coherence as one photomultiplier was moved, with respect to another, across an optical field due to the superposition of the light from two independent thermal light sources, was performed.

The historical and theoretical backgrounds to the experiment are given, and the theoretical equations, describing the effect, are derived in terms of the parameters of the equipment and the geometry of the experiment.

The pair of source apertures were illuminated by the 5461 A and the 4358 A lines, in turn, of an electrodeless Mercury-198 discharge tube. The time-delays between arrivals of photons at the photocathodes of two photomultipliers were recorded by a Time-to-Amplitude Converter and a Pulse-Height Analyser, and the ratio of the number of correlated coincidences, those having a zero time-delay, to the number of random coincidences, those having a time-delay greater than the response time of the detection system, was calculated. Delayed coincidence spectra were obtained at various photomultiplier separations, in a plane parallel to the plane of the sources, for both spectral lines.

The theoretical and experimental values of the correlation ratios are compared, and it is concluded that the two are in good agreement, within the limits of accuracy of the experiment.

CHAPTER 1

Introduction

The theory of coherence is, in general, concerned with the statistical description of the electromagnetic field, and only emerged in its present form, in the nineteen-sixties, when new types of optical field became available with the development of masers and lasers. Before the advent of lasers the theory was mainly concerned with the interference and diffraction phenomena associated with thermal sources.

The first investigation of partial coherence was undertaken by Verdet [1] (1865), who showed the inadequacy of describing light as ideally coherent or ideally incoherent. He observed the interference pattern produced by the light from two pinholes illuminated by the sun, and determined the maximum separation of the pinholes which would still produce visible fringes.

Fizeau [2] (1868) and Michelson [3] (1890) suggested the possibility of using fringe visibility measurements to determine the angular diameters of stars, and later Michelson [4] (1891) also established the connection between the visibility of interference fringes and the energy distribution in a spectral line.

The high-point of the first-order theory came with the van Cittert-Zernike theorem (van Cittert [5] (1934), Zernike [6] (1938)), which is an expression for the correlation between the complex amplitudes of the field variables at two points in the field.

After further work by Hopkins [7] (1951), [8] (1953) [9][10] (1957), Wolf [11] (1954) [12] (1955) [13] (1959), Blanc-Lapierre and Dumontet [14] (1955), Dumontet [15] (1956), Pancharatnam [16] (1956) [17] (1957) [18] (1963), and others, the theory had become fully developed in terms of the correlations between the field variables at two space-time points, and the dynamical laws governing these correlations.

The first measurements of higher order optical correlation effects were carried out by Hanbury-Brown and Twiss [19] (1956) [20] (1957), who demonstrated the existence of a correlation between the intensity fluctuations at two points in the field due to a thermal source. These experiments involved correlating the fluctuations in the currents at the outputs of two photomultipliers placed in two partially coherent optical fields emanating from a single source. More directly, several workers, Twiss, Little and Hanbury-Brown [21] (1957), Rebka and Pound [22] (1957), Brannen, Ferguson and Wehlau [23] (1958) and Twiss and Little [24] (1959), measured the correlation between pulses at the outputs of two photomultipliers in a thermal field.

The full importance of the Hanbury-Brown and Twiss experiments, which had originally been conceived as a method of measuring the angular diameters of visible stars, was not at first appreciated because only thermal sources were used, and these are completely characterised by their first-order correlations. However, with the development of the new types of light sources, it became apparent that, in general, a knowledge of correlation effects of all orders was necessary for the complete statistical description of an optical field. Wolf [25] (1963) [cf. also Mandel [26] (1964), Wolf [27] (1964)] proposed a general classical description, including coherence effects of all orders, in terms of the theory of stochastic processes, and a parallel quantum mechanical theory, in which the quantum correlation functions are expectation values of normally ordered products of the annihilation and creation operators, was developed by Glauber [28][29][30] (1963). In 1965, Titulaer and Glauber [31] proved that a radiation field which gave full fringe contrast, but no Hanbury-Brown and Twiss intensity correlation, was fully coherent, i.e. corresponded to a monochromatic constant amplitude, sinusoidal signal, thus showing the importance of the Hanbury-Brown and Twiss experiments.

On a more particular level, Wolf [32] (1958) proposed a definition of the coherence time in terms of the second-order correlations, while Mandel [33] (1959) proposed a definition of the coherence length in terms of the extent of the unit cell of phase-space in the direction of the light beam. Also, Mandel [34] (1961) [35] (1962) identified the degeneracy as being the average number of photons in a single cell of phase-space, and Kastler [36] (1964) showed that a coherence volume effectively defines a single mode of the radiation field.

Since information about the statistics of optical fields is usually obtained using photoelectric detectors, it was necessary to develop a theory of the photoelectric detection process. Mandel, Sudarshan and Wolf [37] (1964) used a semi-classical approach to show that the correlations between the field variables are related to correlations between photoelectrons, and their results were paralleled by a detailed quantum theory of the single-atom photodetector, put forward by Glauber [38] (1965).

In the early days the Hanbury-Brown and Twiss effect produced a controversy, some workers claiming that a positive correlation would violate fundamental quantum mechanical principles. However, others were able to show that the effect was quantitatively describable in quantum mechanical terms and, in 1957, Silitto [39] and Hanbury-Brown and Twiss [40] pointed out that, in fact, most observable effects could be described by both the wave and the photon theories of light. Sudarshan [41][42] (1963) showed that, by using the diagonal representation of the density operator obtained by introducing the coherent states, obtained by himself and Glauber [28][29][30], it was possible to study the relation between the quantum and classical descriptions of the statistical properties of optical fields. In this representation, the classical and quantum correlation functions are formally equivalent if a generalised phase-space distribution is introduced. [cf. also Mandel and Wolf [43] (1966)].

A method of studying the temporal coherence properties of thermal light was proposed by Mandel[44] (1963), who suggested a measurement of the coherence time, and hence the spectral width, by splitting the output from a single photomultiplier and inserting a variable delay in one of the paths to a coincidence counter. The experiment was successfully performed by Morgan and Mandel[45] (1966) using the blue Mercury-198 spectral line. A similar experiment was performed by Arecchi, Gatti, and Sona[46](1966) using a laser, which showed no correlation, and a pseudothermal source of Gaussian frequency distribution, obtained by passing laser light through a rotating ground-glass screen, which showed a correlation in good agreement with theory. Scarl[47](1966)[48](1968) improved the Hanbury-Brown and Twiss type of experiment by feeding the outputs from the two photomultipliers into a Time-to-Amplitude converter, thus eliminating the need to measure random and correlated count-rates separately.

It was thought that, in order to completely determine the statistical properties of an optical field, a large number of correlation experiments would have to be performed, in order to determine the higher order correlation functions. This was proved to be unnecessary by the work of Wolf and Mehta[49] (1964), who proved that the probability distribution of the intensity of a single mode of the radiation field could be recovered from the photon-counting distribution for that mode.

An expression for the photon-counting distribution, showing that the variance of fluctuations in the number of photoelectrons is the sum of the fluctuations in the number of classical particles obeying Poisson statistics, and of the fluctuations in the classical wave field, was obtained in terms of the integrated intensity by Mandel[50]

(1958)[51] (1959)[52] (1963). The quantum mechanical photon-counting distribution was first derived by Kelly and Kleiner[53] (1964), and their results substantiated the semi-classical derivation of Mandel.

The calculation of the photon-counting distribution for thermal sources of various line shapes under multi-mode conditions is a difficult theoretical problem. Bédard[54] (1966) derived the photon-counting distribution for thermal radiation with a Lorentz line shape, and Srinivasan and Sukuvanam[55] (1972) for thermal radiation of arbitrary line shape. Bédard's predictions were verified by Jakeman and Pike[54] (1968) using a pseudothermal source, obtained by scattering laser light from polystyrene spheres suspended in water.

Saleh[57] (1975) used the methods developed by workers in this field to derive an expression for the second-order coherence function for chaotic light of Gaussian frequency distribution.

Theoretical and experimental work on the photon-counting distribution has led to a detailed study of very narrow spectral lines, and there now exist sophisticated techniques for obtaining information about optical spectra. However, that is beyond the scope of this thesis.

A number of experiments on the interference of independent light beams have been performed. The first of these was by Forrester, Gudmundsen and Johnson[58] (1955), who detected beats between the two components of a Zeeman doublet, and since then several workers have performed similar, but easier because of the much longer coherence time, experiments using two separate lasers, or two modes of the same laser [Javan, Ballik and Bond[59] (1962), Lipsett and Mandel[60] (1963)]. Radloff[61] (1968)[62] (1971) also performed a similar

temporal interference experiment, but under conditions of very low intensity so that the mean time interval between photons was large compared with their transit time through the apparatus, thus demonstrating the interference of a photon with itself.

Transient spatial interference between independant sources has also been observed. Magyar and Mandel[63] (1963) were able to photograph fringes obtained by the superposition of two laser beams, and Haig and Sillitto[64] (1968) [also Haig[65] (1968)] had partial success in measuring the spatial modulation in the mutual coherence pattern when two independent thermal beams were superposed. Again, this type of experiment was performed under conditions of very low intensity [Pfleegor and Mandel[66][67] (1967)[68] (1968)]

A slightly different type of experiment was performed by Sillitto and Wykes[69] (1972) who observed interference between two beams which were alternately transmitted and cut off in anti-phase. This experiment, too, was performed using very low intensities and, as expected, fringes were only observed when the switching frequency was higher than the reciprocal coherence time of the light.

In recent years much thought has been given to the problem of creating and observing non-classical states of the radiation field. A beam having a degree of second-order coherence less than one would be such a state, and could be observed as a decorrelation in a Hanbury-Brown and Twiss type of experiment. That a coherent or chaotic beam undergoing two-photon absorption would become anti-bunched was predicted theoretically by Chandra and Prakash[70] (1970), and the process was studied in detail by Weber[71] (1971), by Simaan and Loudon[72] (1975) and by Every[73] (1975). Weber showed that,

classically, the degree of second-order coherence had a minimum of unity, and using a quantum statistical approach, Simaan and Loudon obtained a minimum of zero. Every found that the time required to achieve an observable effect was prohibitively long.

In 1974, Clauser[74] performed a coincidence counting experiment, on radiating atoms in cascade, which gave strong evidence for the quantum description. In the same year, Stoler[75] suggested second-harmonic generation as a practicable means of producing an observable anti-bunching effect, but so far an experiment of this type has not been performed.

Carmichael and Walls[76] (1976) suggested resonance fluorescence as a means of producing an anti-bunched field, and the experiment was performed by Kimble, Dagenais and Mandel[77] (1977), who claimed to have observed anti-bunching in the radiation emitted by a dilute beam of two-level atoms in the presence of a continuous exciting field. However, Jakeman, Pike, Pusey and Vaughan[78] (1977) pointed out that one had to be certain that only one atom at a time was radiating in order to be able to interpret the experimental results as showing a decorrelation, and that, since the atoms obeyed Poisson statistics, this condition was not satisfied.

The experiment which is the subject of this thesis was a repeat of the Haig and Sillitto[64] experiment, in which the spatial modulation of the intensity correlation, due to the superposition of the light from two independent thermal sources, was observed. The only partial success of the Haig and Sillitto experiment was due to the necessity, when using a coincidence counting technique, of having to measure the correlated and random coincidence count-rates separately, while it is

very difficult to ensure that the intensity of the light does not vary during the two measurement periods. The detector system was improved by using a Time-to-Amplitude Converter with a Pulse-Height-Analyser in place of the coincidence circuits.

CHAPTER 2

The Theory of Optical Coherence

Section (a) The Photoelectric Effect

It is convenient to begin a consideration of the quantum mechanical theory of coherence by a treatment of the photoelectric effect since the detection of optical fields by this process is of central importance to the development of the theory.

It is sufficient to consider only the very simple case of a single atom photodetector in an optical field, and if we work with the electric dipole approximation, standard first-order time-dependent perturbation theory shows that the transition probability per unit time is proportional to:

$$|\hat{\underline{p}}.\hat{\underline{E}}(\underline{r},t)|^2$$

where $\hat{\underline{p}}$ is the electric dipole operator and:

$$\hat{\underline{E}}(\underline{r},t) = \hat{\underline{E}}^{+}(\underline{r},t) + \hat{\underline{E}}^{-}(\underline{r},t) \qquad (1)$$

is the electric field operator; $\hat{\underline{E}}^{+}$ and $\hat{\underline{E}}^{-}$ are the annihilation and creation components of the electric field operator. We will assume that the light is plane polarised in a direction defined by the unit vector $\underline{\epsilon}$, so that we may write:

$$\hat{\underline{E}}(\underline{r},t) = \underline{\epsilon}\,\hat{E}(\underline{r},t) = \underline{\epsilon}\left[\hat{E}^{+}(\underline{r},t) + \hat{E}^{-}(\underline{r},t)\right]$$

If now we consider a transition from the ground state, $|g\rangle$, of the atom to an excited state, $|a\rangle$, associated with a transition of the radiation field from an initial state, $|i\rangle$, to a final state, $|f\rangle$, the transition probability per unit time will be proportional to:

$$|\langle a|\hat{\underline{p}}.\underline{\epsilon}|g\rangle|^2 |\langle f|\hat{E}^{+}(\underline{r},t) + \hat{E}^{-}(\underline{r},t)|i\rangle|^2$$

Since we are considering a process which removes energy from the electromagnetic field only the annihilation component of the electric field operator will have a non-zero matrix element. Thus, using the relation:

$$\langle f|\hat{E}^{+}(\underline{r},t)|i\rangle^{*} = \langle i|\hat{E}^{-}(\underline{r},t)|f\rangle \qquad (2)$$

the transition probability per unit time will be proportional to:

$$|\langle a|\hat{\underline{D}}.\underline{\epsilon}|g\rangle|^{2}\langle i|\hat{E}^{-}(\underline{r},t)|f\rangle\langle f|\hat{E}^{+}(\underline{r},t)|i\rangle$$

Since the states $|f\rangle$ are never observed in practice we must sum over all states $|f\rangle$. Using the completeness relation:

$$\sum_{f}|f\rangle\langle f| = 1 \qquad (3)$$

we obtain that the transition probability per unit time is proportional to:

$$|\langle a|\hat{\underline{D}}.\underline{\epsilon}|g\rangle|^{2}\langle i|\hat{E}^{-}(\underline{r},t)\,\hat{E}^{+}(\underline{r},t)|i\rangle$$

The most we know about the initial states $|i\rangle$ is their probability distribution, so we must also sum over the states $|i\rangle$ weighted by their probabilities P_i, giving:

$$|\langle a|\hat{\underline{D}}.\underline{\epsilon}|g\rangle|^{2}\sum_{i}P_{i}\langle i|\hat{E}^{-}(\underline{r},t)\,\hat{E}^{+}(\underline{r},t)|i\rangle$$

$$= |\langle a|\hat{\underline{D}}.\underline{\epsilon}|g\rangle|^{2}\,\mathrm{Tr}(\hat{\rho}\hat{E}^{-}(\underline{r},t)\,\hat{E}^{+}(\underline{r},t))$$

where $\hat{\rho}$ is the density operator.

Writing the transition probability per unit time between atomic states as P_{ga}, we then find that:

$$P_{ga} = \text{constant} \times |\langle a|\hat{\underline{D}}.\underline{\epsilon}|g\rangle|^{2}\,G^{(1)}(\underline{r}t,\underline{r}t) \qquad (4)$$

where $$G^{(1)}(\underline{r}t,\underline{r}t) = \mathrm{Tr}(\hat{\rho}\,\hat{E}^{-}(\underline{r},t)\,\hat{E}^{+}(\underline{r},t)) \qquad (5)$$

is a correlation function. We may now write the probability for detecting a single photoelectron in a time Δt as:

$$p(1,t) = S\, G^{(1)}(\underline{r}t,\underline{r}t)\, \Delta t \qquad (6)$$

provided that Δt is short enough to ensure that $G^{(1)}$ remains constant over this interval. S is a constant related to the quantum efficiency.

Similarly, the transition probability per unit (time)^2 for the absorption of a photon at $(\underline{r}_1,t_1)$ and a second photon at $(\underline{r}_2,t_2)$ can be shown to be proportional to:

$$\sum_f |\langle f|\hat{E}^+(\underline{r}_1,t_1)\,\hat{E}^+(\underline{r}_2,t_2)|i\rangle|^2$$

where again, since we are removing energy from the field, only the $\hat{E}^+$ operators contribute non-vanishing matrix elements. By the same proceedure as above, this expression becomes:

$$\mathrm{Tr}(\hat{\rho}\,\hat{E}^-(\underline{r}_1,t_1)\,\hat{E}^-(\underline{r}_2,t_2)\,\hat{E}^+(\underline{r}_2,t_2)\,\hat{E}^+(\underline{r}_1,t_1))$$
$$= G^{(2)}(\underline{r}_1t_1,\underline{r}_2t_2,\underline{r}_2t_2,\underline{r}_1t_1) \qquad (7)$$

Thus the photon counting rates are determined by the correlations between the field operators.

Section (b) Two Beam Interference

We will now consider an interference experiment of the Young's double-slit type using plane-polarised quasimonochromatic light.

If the density operator, $\hat{\rho}$, represents the combined field due to two light beams emanating from two pinholes P_1 and P_2, then the expectation value of the intensity at $(\underline{r},t)$ will be given by:

$$\langle I(\underline{r},t)\rangle = \mathrm{Tr}(\hat{\rho}\,\hat{E}^{-}(\underline{r},t)\,\hat{E}^{+}(\underline{r},t)) \tag{8}$$

$\hat{E}^{+}(\underline{r},t)$ may be expressed in terms of the annihilation operators $\hat{a}_k$ for photons of momentum $\hbar\underline{k}$ in the form:

$$\hat{E}^{+}(\underline{r},t) = i\sum_k \left(\frac{\hbar\omega_k c}{V}\right)^{\frac{1}{2}} \hat{a}_k \exp i(-\omega_k t + \underline{k}.\underline{r}) \tag{9}$$

and similarly:

$$\hat{E}^{-}(\underline{r},t) = -i\sum_k \left(\frac{\hbar\omega_k c}{V}\right)^{\frac{1}{2}} \hat{a}_k^{+} \exp i(\omega_k t - \underline{k}.\underline{r}) \tag{10}$$

where the $\hat{a}_k$ and $\hat{a}_k^{+}$ obey the commutation relations:

$$\left[\hat{a}_k, \hat{a}_{k'}\right] = \left[\hat{a}_k^{+}, \hat{a}_{k'}^{+}\right] = 0 \tag{11}$$

$$\left[\hat{a}_k, \hat{a}_{k'}^{+}\right] = \delta_{kk'} \tag{12}$$

If $\hat{\rho}$ is expressed in terms of the coherent states $|\alpha\rangle$ which are eigenstates of the operator $\hat{a}_k$ having eigenvalues α_k, so that

$$\hat{a}_k |\alpha_k\rangle = \alpha_k |\alpha_k\rangle \tag{13}$$

then it can be seen that the operators $\hat{E}^{+}(\underline{r},t)$ and $\hat{a}_k$ are closely related to the complex fields $V(\underline{r},t)$ and their Fourier series complex amplitudes, where $V(\underline{r},t)$ represents the classical complex analytic signal (Born and Wolf[79], 1965). For consider the state:

$$|\{\alpha_k\}\rangle = \prod_k |\alpha_k\rangle \tag{14}$$

We have:

$$\hat{E}^{+}(\underline{r},t)\,|\{\alpha_k\}\rangle = i\sum_k \left(\frac{\hbar\omega_k c}{V}\right)^{\frac{1}{2}} \alpha_k \exp i(-\omega_k t + \underline{k}.\underline{r})\,|\{\alpha_k\}\rangle$$

$$= V(\underline{r},t)\,|\{\alpha_k\}\rangle \tag{15}$$

So the complex analytic wave amplitude $V(\underline{r},t)$ defined by:

$$V(\underline{r},t) = i\sum_k \left(\frac{\hbar\omega_k c}{V}\right)^{\frac{1}{2}} \alpha_k \exp i(-\omega_k t + \underline{k}.\underline{r}) \tag{16}$$

is an eigenvalue of the operator $\hat{E}^{+}(\underline{r},t)$.

The coherent states $|\alpha\rangle$ can be expressed as a Poisson distribution over the number states $|n\rangle$, and, although they are not orthogonal and form an overcomplete set, they satisfy a closure relation of the form:

$$\hat{1} = \prod_k \pi^{-1} \int |\alpha_k\rangle\langle\alpha_k| \, d^2\alpha_k \tag{17}$$

where $d^2\alpha_k$ indicates an integration over the complex α_k plane.

Representing the state of the beam emanating from one pinhole by the basis $|\{\alpha_k'\}\rangle$, and that emanating from the other pinhole by the basis $|\{\alpha_k''\}\rangle$, and describing the probability distribution of the field over the states $|\{\alpha_k'\}\rangle$ and $|\{\alpha_k''\}\rangle$ by the function $P(\{\alpha_k'\},\{\alpha_k''\})$, the density operator may be expressed in the form:

$$\hat{\rho} = \iint P(\{\alpha_k'\},\{\alpha_k''\}) \, |\{\alpha_k'\},\{\alpha_k''\}\rangle\langle\{\alpha_k'\},\{\alpha_k''\}| \, d^2\{\alpha_k'\} \, d^2\{\alpha_k''\} \tag{18}$$

Since the beams emanating from the two pinholes are inclined at a slight angle, they do not share any common $\underline{k}$ mode.

On substituting equation (18) into equation (8) we obtain:

$$\langle I(\underline{r},t)\rangle = \mathrm{Tr} \iint P(\{\alpha_k'\},\{\alpha_k''\}) \, |\{\alpha_k'\},\{\alpha_k''\}\rangle\langle\{\alpha_k'\},\{\alpha_k''\}| \times \hat{E}^{-}(\underline{r},t) \, \hat{E}^{+}(\underline{r},t) \, d^2\{\alpha_k'\} \, d^2\{\alpha_k''\} \tag{19}$$

Now $\hat{E}^{-}(\underline{r},t)$ is the negative frequency operator for the combined field, so that:

$$\langle\{\alpha_k'\},\{\alpha_k''\}| \, \hat{E}^{-}(\underline{r},t) = (V'^{*}(\underline{r},t) + V''^{*}(\underline{r},t)) \, \langle\{\alpha_k'\},\{\alpha_k''\}| \tag{20}$$

Therefore, since the trace is invariant under cyclic permutation of the operators, we obtain:

$$\langle I(\underline{r},t)\rangle = \iint P(\{\alpha'_k\},\{\alpha''_k\})[V'^*(\underline{r},t) + V''^*(\underline{r},t)]$$

$$x[V'(\underline{r},t) + V''(\underline{r},t)]\ d^2\{\alpha'_k\}\ d^2\{\alpha''_k\} \qquad (21)$$

Suppose we are dealing with a stationary field of thermal radiation. The integral can then be interpreted as defining an ensemble average and we may write:

$$\langle I(\underline{r},t)\rangle = \langle [V'^*(\underline{r},t) + V''^*(\underline{r},t)]\,[V'(\underline{r},t) + V''(\underline{r},t)]\rangle \qquad (22)$$

If we express $V'(\underline{r},t)$ and $V''(\underline{r},t)$ in terms of the values at the pinholes at $\underline{r}_1$ and $\underline{r}_2$, i.e. if we set:

$$V'(\underline{r},t) = K_1\ V(\underline{r}_1,t-t_1)$$

$$V''(\underline{r},t) = K_2\ V(\underline{r}_2,t-t_2) \qquad (23)$$

and expand equation (22), we obtain:

$$\langle I(\underline{r},t)\rangle = |K_1|^2\langle I(\underline{r}_1,t-t_1)\rangle + |K_2|^2\langle I(\underline{r}_2,t-t_2)\rangle$$

$$+ 2\mathrm{Re}\left[K_1^*\,K_2\,\Gamma(\underline{r}_1,\underline{r}_2,t-t_1,t-t_2)\right] \qquad (24)$$

The factors K_1 and K_2 depend upon the sizes of the pinholes and on the geometry of the experiment, and are inversely proportional to the distances $(\underline{r}-\underline{r}_1)$ and $(\underline{r}-\underline{r}_2)$.

$$\Gamma(\underline{r}_1,\underline{r}_2,t_1,t_2) = \langle V^*(\underline{r}_1,t_1)\ V(\underline{r}_2,t_2)\rangle \qquad (25)$$

and $\langle I(\underline{r}_j,t_j)\rangle = \langle V^*(\underline{r}_j,t_j)\ V(\underline{r}_j,t_j)\rangle$

$$= \Gamma(\underline{r}_j,\underline{r}_j,t_j,t_j) \qquad j = 1,2 \qquad (26)$$

$\Gamma(\underline{r}_1,\underline{r}_2,t_1,t_2)$ represents the correlation between the field at $(\underline{r}_2,t_2)$ and the complex conjugate field at $(\underline{r}_1,t_1)$ and it will be shown that it is this correlation function which is normally responsible for the sinusoidal modulation of the average intensity

$\langle I(\underline{r},t)\rangle$ with $\underline{r}$.

Since we assume the field to be stationary, the ensemble averages become time-independent and we may shift the origin of time giving:

$$\Gamma(\underline{r}_1,\underline{r}_2,\tau) = \langle V^*(\underline{r}_1,t)\, V(\underline{r}_2,t+\tau)\rangle$$

$$= \lim_{T\to\infty} \frac{1}{2T} \int_{-T}^{T} V^*(\underline{r}_1,t)\, V(\underline{r}_2,t+\tau)\, dt \qquad (27)$$

where $\tau = t_1 - t_2$

and equation (24) becomes:

$$\langle I(\underline{r},t)\rangle = |K_1|^2 \langle I(\underline{r}_1,t)\rangle + |K_2|^2 \langle I(\underline{r}_2,t)\rangle$$

$$+ 2\mathrm{Re}\left[K_1^* K_2\, \Gamma(\underline{r}_1,\underline{r}_2,\tau)\right] \qquad (28)$$

The correlation function $\Gamma(\underline{r}_1,\underline{r}_2,\tau)$ is known as the mutual coherence function. It is convenient to normalise Γ by setting:

$$\gamma(\underline{r}_1,\underline{r}_2,\tau) = \frac{\Gamma(\underline{r}_1,\underline{r}_2,\tau)}{[\Gamma(\underline{r}_1,\underline{r}_1,0)]^{\frac{1}{2}}\ [\Gamma(\underline{r}_2,\underline{r}_2,0)]^{\frac{1}{2}}}$$

$$= \frac{\Gamma(\underline{r}_1,\underline{r}_2,\tau)}{\langle I(\underline{r}_1)\rangle^{\frac{1}{2}} \langle I(\underline{r}_2)\rangle^{\frac{1}{2}}} \qquad (29)$$

We can now write:

$$\langle I(\underline{r},t)\rangle = \langle I_1(\underline{r},t)\rangle + \langle I_2(\underline{r},t)\rangle + 2\langle I_1(\underline{r},t)\rangle^{\frac{1}{2}}$$

$$\times \langle I_2(\underline{r},t)\rangle^{\frac{1}{2}}\, \mathrm{Re}\left[\gamma(\underline{r}_1,\underline{r}_2,(\tfrac{s_1 - s_2}{c}))\right] \qquad (30)$$

where we have introduced the intensity:

$$I_j(\underline{r},t) = |K_j|^2\, I(\underline{r}_j,t) \qquad (31)$$

at $(\underline{r},t)$ arising from pinhole P_j alone.

From this equation it is apparent that values for the real parts of $\gamma(\underline{r}_1,\underline{r}_2,\tau)$ may be obtained from intensity measurements in an

interference experiment. However, it is the absolute value of the normalised complex correlation function γ, rather than just its real part, which is a true measure of the sharpness of the interference effects.

If ν_o is the effective frequency of the light, assumed quasi-monochromatic, we may write:

$$\gamma(\underline{r}_1,\underline{r}_2,\tau) = |\gamma(\underline{r}_1,\underline{r}_2,\tau)| \exp\{i\,[\alpha(\underline{r}_1,\underline{r}_2,\tau) - 2\pi\nu_o\tau]\} \qquad (32)$$

where $$\alpha(\underline{r}_1,\underline{r}_2,\tau) = \arg\gamma(\underline{r}_1,\underline{r}_2,\tau) + 2\pi\nu_o\tau \qquad (33)$$

Equation (30) then becomes:

$$\langle I(\underline{r},t)\rangle = \langle I_1(\underline{r},t)\rangle + \langle I_2(\underline{r},t)\rangle + 2\langle I_1(\underline{r},t)\rangle^{\frac{1}{2}}\langle I_2(\underline{r},t)\rangle^{\frac{1}{2}} \times |\gamma(\underline{r}_1,\underline{r}_2,\tfrac{(s_1-s_2)}{c})| \cos\left[\alpha(\underline{r}_1,\underline{r}_2,\tfrac{(s_1-s_2)}{c}) - \delta\right] \qquad (34)$$

where $$\delta = 2\pi\nu_o\left(\frac{s_1-s_2}{c}\right) = \frac{2\pi}{\lambda_o}(s_1-s_2) \qquad (35)$$

In general, due to the small effective wavelength, λ_o, the cosine term in equation (34) will vary much more rapidly with position $\underline{r}$, across the field, than the other terms in the equation. The depth of the modulation is an observable in any interference experiment, and, following Michelson, we define it as the visibility $U(\underline{r})$ at the point $P(\underline{r})$, where:

$$U(\underline{r}) = \frac{\langle I\rangle_{max} - \langle I\rangle_{min}}{\langle I\rangle_{max} + \langle I\rangle_{min}} \qquad (36)$$

and $\langle I\rangle_{max.}$ and $\langle I\rangle_{min.}$ are the maximum and minimum intensities near $P(\underline{r})$. To a good approximation, the maximum and minimum values of the intensity can be obtained by setting the cosine to ± 1 in equation (34), and we get:

$$U(\underline{r}) = \frac{2\langle I_1(\underline{r},t)\rangle^{\frac{1}{2}}\langle I_2(\underline{r},t)\rangle^{\frac{1}{2}}}{\langle I_1(\underline{r},t)\rangle + \langle I_2(\underline{r},t)\rangle} \; |\gamma(\underline{r}_1,\underline{r}_2,\tfrac{(s_1-s_2)}{c})| \qquad (37)$$

In particular if $\langle I_1\rangle = \langle I_2\rangle$ then:

$$U(\underline{r}) = |\gamma(\underline{r}_1,\underline{r}_2,\tfrac{(s_1-s_2)}{c})| \qquad (38)$$

in which case the visibility of the interference fringes becomes a direct measure of $|\gamma_{12}|$. The argument of γ_{12} determines the positions of the fringes in the plane of the locus of point P. The positions of the maxima in the interference pattern are given by:

$$\arg \gamma(\underline{r}_1,\underline{r}_2,\tfrac{(s_1-s_2)}{c})) = \alpha(\underline{r}_1,\underline{r}_2,\tfrac{(s_1-s_2)}{c})) - 2\pi\tfrac{(s_1-s_2)}{\lambda_o}$$

$$= 2m \qquad (m=0,1,2.....) \qquad (39)$$

We have seen that γ_{12} is determined by the ability of the light from points P_1 and P_2 to interfere at the point $P(\underline{r})$, and γ_{12} is therefore termed the complex degree of first-order coherence of the field at the points P_1 and P_2.

Normalisation ensures that $|\gamma_{12}| \leqslant 1$. The extreme value unity would be obtained with a constant-amplitude sine-wave of wavelength λ_o, and with the phase difference, δ, between the vibrations at P_1 and P_2 equal to $\alpha(\underline{r}_1,\underline{r}_2,(s_1-s_2)/c)$. A beam having $|\gamma_{12}| = 1$ is said to be completely first-order coherent at the points P_1 and P_2. A spread of wavelengths will blur the fringes at $P(\underline{r})$ and thus, in general, a non-monochromatc chaotic beam has $|\gamma_{12}| < 1$, unless $\underline{r}_1 = \underline{r}_2$ and $s_1 = s_2$, in which case $|\gamma_{12}|$ again reaches the value unity. If $\underline{r}_1 = \underline{r}_2$, as, for example, in a Michelson Interferometer, a coherence length can be defined as the maximum difference between

s_1 and s_2 at which interference fringes are still produced. Also, a coherence area may be defined in terms of the maximum lateral separation of P_1 and P_2, with $s_1 = s_2$, at which interference fringes may still be observed. Combining these two, we may define a coherence volume such that any two points contained within a single coherence volume have $|\gamma_{12}| > 0$, and any two points not contained within a single coherence volume have $|\gamma_{12}| = 0$.

Section (c) Intensity Correlation

In this section we shall show that if we place two photodetectors at points P_1 and P_2 in an optical field, and if there are fluctuations in the intensity of the field, then these fluctuations will be measurable in terms of a correlation between the fluctuations in the outputs of the detectors, provided there is some coherence between the light at P_1 and P_2.

Using the left-hand-side of equation (7), and following the procedure of the previous section, we can write:

$$\langle I(\underline{r}_1, t+\tau)\, I(\underline{r}_2, t)\rangle = \mathrm{Tr}\big(\hat{\rho}\,\hat{E}^-(\underline{r}_1, t+\tau)\,\hat{E}^-(\underline{r}_2, t) \times \hat{E}^+(\underline{r}_2, t)\,\hat{E}^+(\underline{r}_1, t+\tau)\big) \qquad (40)$$

and can obtain:

$$\langle I(\underline{r}_1, t+\tau)\, I(\underline{r}_2, t)\rangle = \langle V(\underline{r}_1, t+\tau)\, V^*(\underline{r}_1, t+\tau)\, V(\underline{r}_2, t)\, V^*(\underline{r}_2, t)\rangle \qquad (41)$$

where V and V^*, being scalars, may be written in any order we please. The amplitudes, V, can be expanded as a superposition of plane wave contributions:

$$V(\underline{r}_1, t+\tau) = \sum_{k} V_k \exp i(-\omega_k(t+\tau) + \underline{k}.\underline{r}_1) \qquad (42)$$

giving:

$$\langle I(\underline{r}_1, t+\tau)\, I(\underline{r}_2, t)\rangle = \sum_{k_1 k_2 k_3 k_4} \langle V^*_{k_1} V^*_{k_2} V_{k_3} V_{k_4}\rangle$$

$$\times \exp\left[i(-\underline{k}_1.\underline{r}_1 + \omega_1(t+\tau) - \underline{k}_2.\underline{r}_2 + \omega_2 t - \underline{k}_3.\underline{r}_2 - \omega_3 t + \underline{k}_4.\underline{r}_1 - \omega_4(t+\tau))\right] \qquad (43)$$

The four complex Fourier coefficients in equation (43) are independent random variables having zero mean-values, and there are only two types of term in the summation for which the ensemble average on the right does not vanish. These arise for:

$$\left.\begin{aligned}\underline{k}_1 &= \underline{k}_3\\ \underline{k}_2 &= \underline{k}_4\end{aligned}\right\} \quad \text{and} \quad \left.\begin{aligned}\underline{k}_1 &= \underline{k}_4\\ \underline{k}_2 &= \underline{k}_3\end{aligned}\right\} \qquad (44)$$

Thus equation (43) simplifies to:

$$\langle I(\underline{r}_1, t+\tau)\, I(\underline{r}_2, t)\rangle = \sum_{k_1 k_2} \langle |V_{k_1}|^2\rangle \langle |V_{k_2}|^2\rangle$$

$$\times \left[\exp\left[i(\omega_1 - \omega_2)\tau_{12}\right] + 1\right] \qquad (45)$$

where $\tau_{12} = \tau - (\underline{r}_1 - \underline{r}_2)/c$

Equation (45) may now be written in terms of the first-order correlation function:

$$\langle I(\underline{r}_1, t+\tau)\, I(\underline{r}_2, t)\rangle = \langle I(\underline{r}_1)\rangle\langle I(\underline{r}_2)\rangle + |\langle V^*(\underline{r}_1, t+\tau)\, V(\underline{r}_2, t)\rangle|^2$$

$$= \langle I(\underline{r}_1)\rangle\langle I(\underline{r}_2)\rangle + |\Gamma(\underline{r}_1, \underline{r}_2, \tau)|^2$$

$$= \langle I(\underline{r}_1)\rangle\langle I(\underline{r}_2)\rangle\left[1 + |\gamma(\underline{r}_1, \underline{r}_2, \tau)|^2\right] \qquad (46)$$

We can then express this result in terms of fluctuation correlations.

If:

$$\Delta I(\underline{r}_1, t+\tau) = I(\underline{r}_1, t+\tau) - \langle I(\underline{r}_1)\rangle$$

and $$\Delta I(\underline{r}_2, t) = I(\underline{r}_2, t) - \langle I(\underline{r}_2)\rangle \qquad (47)$$

then:

$$\langle \Delta I(\underline{r}_1, t+\tau)\, \Delta I(\underline{r}_2, t)\rangle = \langle I(\underline{r}_1, t+\tau)\, I(\underline{r}_2, t)\rangle - \langle I(\underline{r}_1)\rangle\langle I(\underline{r}_2)\rangle$$

$$= \langle I(\underline{r}_1)\rangle\langle I(\underline{r}_2)\rangle\, |\gamma(\underline{r}_1, \underline{r}_2, \tau)|^2 \qquad (48)$$

Hence:

$$\langle I(\underline{r}_1, t+\tau)\, I(\underline{r}_2, t)\rangle = \langle I(\underline{r}_1)\rangle\langle I(\underline{r}_2)\rangle\, (1 + |\gamma(\underline{r}_1, \underline{r}_2, \tau)|^2) \qquad (48a)$$

Then if we define the degree of second-order coherence by:

$$\gamma^{(2)}_{12}(\underline{r}_1, \underline{r}_2, \tau) = \frac{\langle I(\underline{r}_1, t+\tau)\, I(\underline{r}_2, t)\rangle}{\langle I(\underline{r}_1)\rangle\langle I(\underline{r}_2)\rangle}\,, \qquad (49)$$

we see that it is determined by the modulus of the corresponding degree of first-order coherence.

If we consider a constant-amplitude sine-wave, then equation (43) simplifies to:

$$\langle I(\underline{r}_1, t+\tau)\, I(\underline{r}_2, t)\rangle = \langle I(\underline{r}_1)\rangle\langle I(\underline{r}_2)\rangle \qquad (49a)$$

so that:

$$\langle \Delta I(\underline{r}_1, t+\tau)\, \Delta I(\underline{r}_2, t)\rangle = 0 \qquad (49b)$$

and $$\gamma^{(2)}_{12}(\underline{r}_1, \underline{r}_2, \tau) = 1$$

Thus a beam which is second-order coherent, i.e. has $\gamma^{(2)}_{12} = 1$, shows no intensity fluctuations. The intensity fluctuations of a chaotic beam are a wave interference effect resulting from the

statistical contributions of a large number of modes to the beam. From the discussion of coherence length at the end of section (b), it can be seen that these fluctuations occur with a time-scale of the order of the coherence time, where the coherence time is the coherence length divided by the velocity of light.

Section (d) Bunching of Photons

By expressing the density operator in terms of the coherent states which are eigenstates of the electric field operators, we were able to obtain an expression for the classical observable intensity in terms of the complex analytic signal. This approach was useful since, historically, coherence was defined in terms of classical waves and quantum coherence was then defined so as to agree with the classical definitions.

In section (c) we showed that a constant-amplitude sine-wave had:

$$\langle I(\underline{r}_1, t+\tau)\, I(\underline{r}_2, t)\rangle = \langle I(\underline{r}_1)\rangle \langle I(\underline{r}_2)\rangle$$

By considering such a wave as exhibiting the greatest possible coherence, the condition for second-order coherence can be expressed as the ability of the second-order correlation function to factorise in this way; i.e. in a field which is second-order coherent, the expectation value of the product of the intensities measured by two photodetectors is equal to the product of the expectation values of the intensities measured by each photodetector separately. By

analogy, in quantum terms, in a field which is second-order coherent, the two-fold coincidence counting rate of two photodetectors is equal to the product of the counting rates measured by each photodetector individually. More formally, we may express the condition for second-order coherence by:

$$G^{(2)}(x_1,x_2,x_2,x_1) = G^{(1)}(x_1,x_1)\, G^{(1)}(x_2,x_2) \tag{50}$$

where $x_1 = (\underline{r}_1, t_1)$.

Consider the first-order correlation function:

$$G^{(1)}(x_1,x_1) = \mathrm{Tr}(\hat{\rho}\, \hat{E}^-(x_1)\, \hat{E}^+(x_1)) \tag{51}$$

is effectively $\langle \hat{a}^+ \hat{a} \rangle = \langle n \rangle$. i.e., the probability for detecting a single photon is proportional to the expectation value of the number of photons in the beam. For a multi-mode beam, the probability is proportional to the expectation value of the sum of the contributions from each mode, which is again just the expectation value of the total number of photons in the beam.

The second-order correlation function, with $x_1 = x_2$, is:

$$G^{(2)}(x_1,x_1,x_1,x_1) = \mathrm{Tr}(\hat{\rho}\, \hat{E}^-(x_1)\, \hat{E}^-(x_1)\, \hat{E}^+(x_1)\, \hat{E}^+(x_1)) \tag{52}$$

which is effectively $\langle \hat{a}^+ \hat{a}^+ \hat{a}\, \hat{a} \rangle = \langle n(n-1) \rangle$, where we have used the commutation relation $\hat{a}^+\hat{a} = \hat{a}\,\hat{a}^+ - 1$ and the definition of the number operator as $\hat{n} = \hat{a}^+\hat{a}$.

Thus a beam which is second-order coherent according to equation (50) has:

$$\langle n(n-1) \rangle = \langle n \rangle^2 \tag{53}$$

which is characteristic of a Poisson distribution over the states $|n\rangle$. For a thermal beam, however, we have:

$$\langle n(n-1)\rangle = \langle n\rangle^2 \left(1 + |\gamma_{12}^{(1)}|^2\right) \qquad (54)$$

where $|\gamma_{12}^{(1)}|^2 \neq 0$ since we have put $x_1 = x_2$. Thus the second-order correlation function for a thermal beam does not satisfy the factorisation condition (50) and the beam is, therefore, not second-order coherent. This is because thermal light obeys Bose-Einstein statistics and can be interpreted as a tendency of the photons to 'bunch'.

If we define an arbitrary volume of space and count the number of photons within that volume, and if we repeat the measurement a large number of times, then, if the light is second-order coherent, the number of photons per volume will fluctuate according to Poissonian statistics. The Poissonian beam is a beam of constant intensity analogous to the classical constant-amplitude sine-wave, and the observed fluctuations may be regarded as due to the discrete nature of the photoelectric process (cf. "shot noise").

If now we perform the same experiment using thermal light, and if the volume is of the order of the coherence volume, then the number of photons per volume will fluctuate in excess of the Poissonian fluctuations. This might be taken to imply that a thermal light source emits photons in bunchs.

Section (e) Propagation Laws

In this section we will derive an expression for the mutual coherence at the photodetectors in terms of the geometry of the system.

In vacuo, the mutual coherence function $\Gamma(P_1,P_2,\tau)$ obeys a wave equation (Wolf[12], 1955). If the field is stationary the equation takes the form:

$$\nabla^2\Gamma = c^{-2}\frac{\partial^2\Gamma}{\partial\tau^2} \tag{55}$$

If S_1 and S_2 are two typical points on the source σ, P_1 and P_2 are two points in the field, $R_1 = S_1P_1$, $R_2 = S_2P_2$ and Θ_1 and Θ_2 are angles which the lines S_1P_1 and S_2P_2 make with the normal to the source, then the solution of the wave equation may be written in the form (Parrent[80][81], 1959):

$$\Gamma(P_1,P_2,\tau) = \frac{1}{(2\pi)^2}\iint \frac{\cos\Theta_1\cos\Theta_2}{R_1^2R_2^2}\, D\,\Gamma(S_1,S_2,\tau-\frac{R_1-R_2}{c})\,dS_1\,dS_2 \tag{56}$$

where D denotes the differential operator:

$$D = 1 + \frac{R_1-R_2}{c}\frac{\partial}{\partial\tau} - \frac{R_1R_2}{c^2}\frac{\partial^2}{\partial\tau^2} \tag{57}$$

dS_1 and dS_2 are elements of the surface of the source, centred on the points S_1 and S_2, and the integration is to be taken twice over the surface of the source.

If σ is an extended thermal source one may assume that the different elements are radiating independently. If, also, the radiation is quasimonochromatic of frequency ν_o then:

$$\Gamma(S_1,S_2,\tau) \sim I(S_1)\,\delta(S_1-S_2)\exp(-2\pi i\,\nu_o\,\tau) \qquad (|\tau| < \frac{1}{\Delta\nu}) \tag{58}$$

where $I(S_1)$ is the intensity at S_1 per unit area of the source.

If moreover, $R_1 \gg \lambda_o$, $R_2 \gg \lambda_o$, the angles Θ_1 and Θ_2 are sufficiently small, and:

$$|\tau - (R_1 - R_2)/c| \ll \frac{1}{\Delta\nu} \tag{59}$$

then equation (56) reduces to:

$$\Gamma(P_1, P_2, \tau) \sim \left(\frac{k_o}{2\pi}\right)^2 \exp(-2\pi i \nu_o \tau) \int \frac{I(S)}{R_1 R_2} \exp[-ik_o(R_1 - R_2)]\, dS \tag{60}$$

This is essentially a rigorous formulation of the van Cittert-Zernike theorem. It is noticeable that this integral is of the same form as the expression for the amplitude in the diffraction pattern of an aperture the same shape as σ, and with an amplitude transmittance proportional to the intensity per unit area in σ, as given by the Fresnel-Kirchhoff theory.

Equation (60) can be simplified further if P_1 and P_2 are in a plane parallel to the plane of the source, and the separation between P_1 and P_2 is small compared with R, the distance between the planes. Under these conditions:

$$\Gamma(P_1, P_2, \tau) \sim \left(\frac{k_o}{2\pi}\right)^2 \frac{\exp[i(\psi - 2\pi\nu_o\tau)]}{R^2} \int_\sigma I(\xi, \eta) \exp[ik_o(p\xi + q\eta)]\, d\xi\, d\eta \tag{61}$$

where $p = (x_2 - x_1)/R$, $\quad q = (y_2 - y_1)/R$ (62)

and $\psi = k_o [(x_2^2 + y_2^2) - (x_1^2 + y_1^2)] /2R$ (63)

(x_1, y_1) and (x_2, y_2) are the coordinates of P_1 and P_2, and (ξ, η) are coordinates of the source point S referred to cartesian axes with directions OX and OY in the plane of the source.

This equation shows that, apart from constant factors, the mutual

coherence function is just the Fourier transform of the average intensity distribution across the source.

Section (f) The Measurement of Photoelectron Pulse Correlations

In the previous sections we have derived the basic equations that are relevant to the experiment that forms the subject of this thesis, but without allowing for the practical effects of e.g. the finite response times of the photodetectors. The experiment was first performed by Haig and Sillitto[64] (1968) (also Haig[65], 1968), and involved the detection of a correlation in the photoelectron coincidence count-rate as one detector was moved, with respect to another, across the field due to a pair of small apertures illuminated by a Mercury-198 lamp. In this section we shall derive expressions for the coincidence count-rate and the signal-to-noise ratio in terms of the experimental variables.

Consider two beams of partially coherent light emanating from a single source, and having average photon arrival rates, N_1' and N_2' photons per second, at two photodetectors P_1 and P_2. Let the pulses be fed into a coincidence circuit having resolving time τ_r. If the quantum efficiencies of P_1 and P_2 are α_1 and α_2 respectively, so that the single channel count-rates of P_1 and P_2 are given by:

$$N_1 = \alpha_1 N_1'$$

$$\text{and} \qquad N_2 = \alpha_2 N_2' \qquad (64)$$

then the coincidence rate will be given by:

$$\bar{C} = 2N_1 N_2 \tau_r \left[1 + \tfrac{1}{2} |\nu_{12}(\underline{r}_1, \underline{r}_2, 0)|^2 \ \zeta(\tau_r)/\tau_r\right] \qquad (65)$$

The factor $2\tau_r$ arises because we have integrated the coincidence rate over the response time of the coincidence circuit, and the second term inside the brackets has been multiplied by $\frac{1}{2}$ because the beam is assumed to be unpolarised and the orthogonal polarisation components are uncorrelated.

$$\zeta(\tau_r) = \int_{-\tau_r}^{\tau_r} |\nu_{11}(\tau)|^2 \, d\tau \qquad (66)$$

The two terms on the right-hand side of equation (65) represent the random and correlated coincidence count-rates.

Since the visibility of fringes, observed using a Michelson Interferometer, is proportional to $|\nu_{11}(\tau)|$, it is evident that one may define a coherence time in terms of $|\nu_{11}(\tau)|$. Thus:

$$|\nu_{11}(\tau)| \sim 0 \text{ for } \tau \gg \tau_o$$

$$|\nu_{11}(\tau)| \sim 1 \text{ for } \tau \ll \tau_o$$

and the coherence time, τ_o, can be defined in terms of ν by:

$$\tau_o = \int_{-\infty}^{\infty} |\nu_{11}(\tau)|^2 \, d\tau \qquad (67)$$

Thus $\zeta(\tau_r) \sim \tau_r$ for $\tau_r \ll \tau_o$, and $\zeta(\tau_r) \sim \tau_o$ for $\tau_r \gtrsim \tau_o$. It is apparent, therefore, that the enhanced coincidence effect will only be measurable for detectors having a very short resolving time and for light sources having a long coherence time. In practice, using a thermal light source, we will have $\tau_r \gtrsim \tau_o$, therefore the second approximation above will hold.

The effect of a finite resolving time is to reduce the

observable correlation. A second effect which contributes to the reduction of the observable correlation is the finite sizes of the source and detector apertures. To take account of this we may factorise $|\gamma_{12}(\underline{r}_1, \underline{r}_2, 0)|^2$ into two parts:

$$|\gamma_{12}(\underline{r}_1, \underline{r}_2, 0)|^2 = \Gamma^2_{12}(d, \nu_o)\, \Delta(\nu_o) \qquad (67a)$$

$\Gamma^2_{12}(d, \nu_o)$ is the correlation which would be measured by point detectors, separated by a distance d, observing the light from a point source, or point sources. $\Delta(\nu_o)$ is the average correlation between all pairs of points on the detectors due to all points on the source; i.e. $\Delta(\nu_o)$ is obtained by integrating $\Gamma^2_{12}(0, \nu_o)$ over each aperture and normalising the result.

It is also necessary to introduce factors, f_1 and f_2, to allow for any loss of correlation due to polarisation effects in the optical system and noise in the photodetectors. These factors will be evaluated later (pages 53 and 55).

In terms of physically measurable quantities we have that the number of random coincidences measured in a time T_o is given by:

$$\overline{C_R(T_o)} = 2 N_o^2 \tau_r T_o \qquad (68)$$

and the number of correlated coincidences is given by:

$$\overline{C_c(T_o)} = \tfrac{1}{2} N_o^2 \tau_o T_o \; \Delta(\nu_o)\, \Gamma^2_{12}(d, \nu_o)\, f_1 f_2 \qquad (69)$$

where it has been assumed that $N_1 = N_2 = N_o$.

Thus, the correlation between the photons arriving at the two photodetectors increases the number of coincidences by a factor:

$$1 + \rho_c = 1 + \tfrac{1}{4} \frac{\tau_o}{\tau_r} \Delta(\nu_o)\, \Gamma^2_{12}(d, \nu_o)\, f_1 f_2 \qquad (70)$$

The quantity that was determined from the experiment was ρ_c, the ratio of the number of correlated coincidences to the number of random coincidences.

The random coincidences obey a Poisson distribution, so the r.m.s. fluctuation in their number is given by:

$$\left[\overline{(C_R(T_o) - \overline{C_R(T_o)})^2}\right]^{\frac{1}{2}} = \overline{C_R(T_o)}^{\frac{1}{2}} \qquad (71)$$

$$= N_o (2\tau_r T_o)^{\frac{1}{2}} \qquad (71)$$

Therefore if the signal-to-noise ratio is defined as the ratio of the average number of correlated coincidences to the r.m.s. fluctuation in the random coincidences, then:

$$S/N = \frac{\overline{C_c(T_o)}}{\overline{C_R(T_o)}^{\frac{1}{2}}} = \tfrac{1}{2} N_o \tau_o \Delta(\nu_o) \Gamma^2_{12}(d,\nu_o) f_1 f_2 \left(\frac{T_o}{2\tau_r}\right)^{\frac{1}{2}} \qquad (72)$$

Thus we have expressions for the ratio of the correlated to random coincidences and the signal-to-noise ratio and it only remains to derive an explicit expression for $\Delta(\nu_o) \Gamma^2_{12}(d,\nu_o)$.

Section (g) The Derivation of $\Delta(\nu_o) \Gamma^2(d,\nu_o)$

Following Haig, we will now derive the value of $\Delta(\nu_o) \Gamma^2(d,\nu_o)$ for this experiment. The source and detector apertures along with their coordinates are illustrated in Fig. 2.1. The source comprises two rectangular apertures of identical shape, size and orientation, disposed in the same horizontal plane as the two rectangular detector apertures. The origin of the rectangular Cartesian coordinate

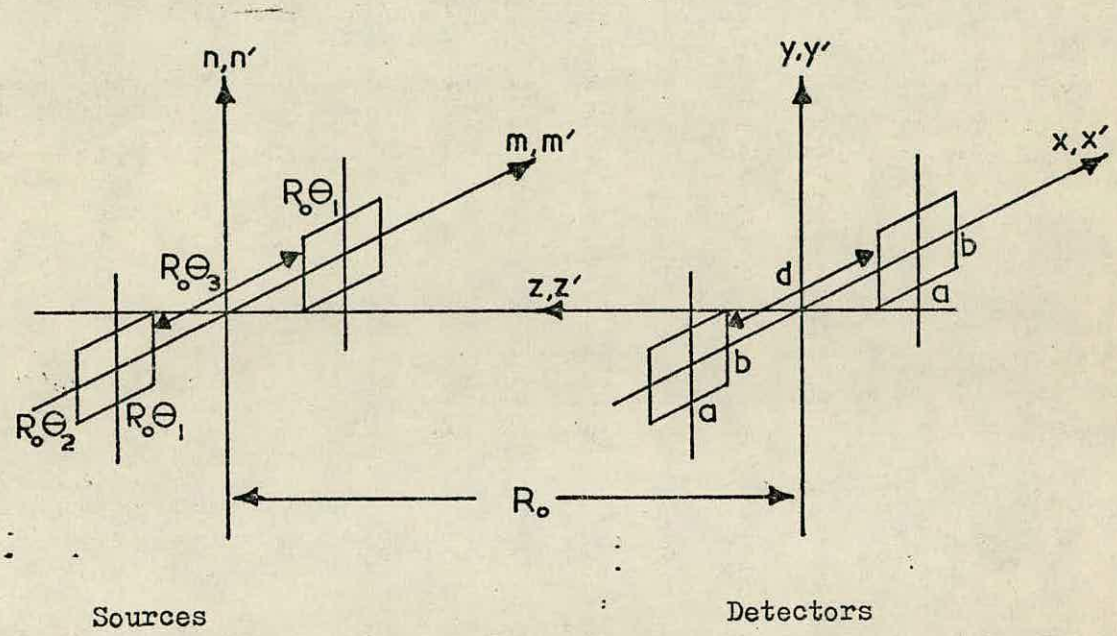

Fig.2.1: Diagram to illustrate the co-ordinate system.

system lies midway between the centres of the two detector apertures. Both detector apertures lie on the x-axis such that the z-axis passes through the midpoint of the line joining the centres of the two source apertures. We assume that the source, distant R_o from the xy-plane, can be divided up into elementary areas, $dM = dmdn$, centred on the points (m,n,R_o). Let m and m' be the coordinates of arbitrary points on the surfaces of the source. $X = (x,y,o)$ are the coordinates of an arbitrary point on the photocathode defined by:

$$-\frac{b}{2} < y < \frac{b}{2} \quad , \quad -\tfrac{1}{2}(d+a) < x < -\tfrac{1}{2}(d-a),$$

and $X' = (x', y', o)$ are the coordinates of an arbitrary point on the other photocathode defined by:

$$-\frac{b}{2} < y' < \frac{b}{2} \quad , \quad \tfrac{1}{2}(d-a) < x' < \tfrac{1}{2}(d+a).$$

The sides of the source are assumed to be parallel to the sides of the detector apertures.

Assuming the Hanbury-Brown and Twiss definition of $\Delta(\nu_o)$ and $\Gamma^2(d, \nu_o)$, it follows that:

$$\Delta(\nu_o)\,\Gamma^2(d,\nu_o) = \frac{1}{\Omega_o^2 A_1 A_2 R_o^4} \iiiint dMdM'\,dXdX' \cdot \cos\left[\frac{2\pi\nu_o(X-X')(M-M')}{cR_o}\right], \qquad (73)$$

where the areas, A_1 and A_2, of the photocathodes, and the solid angle, Ω_o, subtended by a source aperture at the photodetectors, are given by:

$$A_1 = \int dX \,, \qquad A_2 = \int dX' \qquad \left.\right\} \tag{74}$$

and $$\Omega_o = \int \frac{dM}{R_o^2} = \int \frac{dM'}{R_o^2} \qquad \left.\right\}$$

(Note: Throughout these successive integrations we will use a compact notation, such that the successive products of cosine terms involving the independent expressions (m-m'), (n-n'), (x-x') and (y-y') are integrated one at a time, implicitly maintaining the remainder constant).

The integrations in equation (73) are taken in four ways:

(i) From left-hand source to left hand detector.

(ii) From left-hand source to right-hand detector.

(iii) From right-hand source to left hand detector.

(iv) From right-hand source to right-hand detector.

Each of the above terms will be treated separately, except in the case of the first few integrations, which are common to all terms.

Taking any one of the four terms, we will integrate over the detector apertures, beginning with the x,x' - direction:

$$\Delta(\nu_o)\,\Gamma^2(d,\nu_o) = \frac{1}{\Omega_o^2 A_1 A_2 R_o^4} \iint dM.dM' \iint dy.dy' \int dx' \cdot \int_{\frac{1}{2}(d-a)}^{\frac{1}{2}(d+a)} \mathrm{Cos}\ \alpha(x-x')dx \tag{75}$$

where $$\alpha = \frac{2\pi\nu_o (M-M')}{cR_o} \,.$$

Simplifying, we have

$$\Delta(\nu_o)\,\Gamma^2(d,\nu_o) = F_1\left[\cos\alpha x' \int_{\frac{1}{2}(d-a)}^{\frac{1}{2}(d+a)} \cos\alpha x\,dx + \sin\alpha x' \cdot \int_{\frac{1}{2}(d-a)}^{\frac{1}{2}(d+a)} \sin\alpha x\,dx\right] \qquad (76)$$

where: $$F_1 = \frac{1}{\Omega_o^{\,2} A_1 A_2 R_o^{\,4}} \iint dM.dM' \iint dy\,dy' \int dx' .$$

and then:

$$\Delta(\nu_o)\,\Gamma^2(d,\nu_o) = F_1\left[\frac{1}{\alpha}\cos\alpha x'\,(2\cos\frac{\alpha d}{2}\sin\frac{\alpha a}{2}) + \frac{1}{\alpha}\sin\alpha x' \cdot (2\sin\frac{\alpha d}{2}\sin\frac{\alpha a}{2})\right].$$

Rearranging, and integrating over x':

$$= F_2\left[\cos\frac{\alpha d}{2}\int_{-\frac{1}{2}(d+a)}^{-\frac{1}{2}(d-a)}\cos\alpha x'dx' + \sin\frac{\alpha d}{2}\int_{-\frac{1}{2}(d+a)}^{-\frac{1}{2}(d-a)}\sin\alpha x'.dx'\right]$$

where

$$F_2 = \frac{1}{\Omega_o^{\,2} A_1 A_2 R_o^{\,4}} \iint dM.dM' \iint dy.dy' \left(\frac{2}{\alpha}\sin\frac{\alpha a}{2}\right).$$

Thus,

$$\Delta(\nu_o)\Gamma^2(d,\nu_o) = F_2\left(\frac{2}{\alpha}\sin\frac{\alpha a}{2}\right)\left[\cos\frac{\alpha d}{2}\cos\frac{-\alpha d}{2} + \sin\frac{\alpha d}{2}\sin\frac{-\alpha d}{2}\right]$$

i.e. $$\Delta(\nu_o)\,\Gamma^2(d,\nu_o) = \frac{1}{\Omega_o^{\,2} A_1 A_2 R_o^{\,4}} \iiiint dM.dM'\,dydy' \cdot \left[\frac{2}{\alpha}\sin\frac{\alpha a}{2}\right]^2 \left[\cos\alpha d\right] \qquad (77)$$

Now, so far we have integrated only over the x and x'- axis of the detector apertures. The integration over the y and y'-axis follows

a precisely similar pattern, apart from the obvious omission of the Cosine modulating term, and so, remembering that $A_1 = A_2 = ab$, we have:

$$\Delta(\nu_o)\,\Gamma^2(d,\nu_o) = \frac{1}{(\theta_1\theta_2)^2 R_o^4}\iint dM.dM' \left[\frac{2\sin\frac{\alpha a}{2}}{\alpha a}\right]^2 \cdot \left[\frac{2\sin\frac{\alpha b}{2}}{\alpha b}\right]^2 \cos \alpha d.$$

Since: $\alpha = \dfrac{2\pi\nu_o(M-M')}{cR_o}$, each term is expressed in full as:

$$= \frac{1}{(\theta_1\theta_2)^2 R_o^4}\iiiint dm.dn.dm'.dn' \left[\frac{\sin\frac{\pi\nu_o a(m-m')}{cR_o}}{\frac{\pi\nu_o a(m-m')}{cR_o}}\right]^2 \cdot \left[\frac{\sin\frac{\pi\nu_o b(n-n')}{cR_o}}{\frac{\pi\nu_o b(n-n')}{cR_o}}\right]^2 \left[\cos\frac{2\pi\nu_o d(m-m')}{cR_o}\right]^2 . \quad (78)$$

At this point it is convenient to change the variables. We therefore put:

$$\phi = \frac{\pi\nu_o a(m-m')}{cR_o} \qquad \phi' = \frac{\pi\nu_o a(m+m')}{2cR_o}$$

$$\psi = \frac{\pi\nu_o b(n-n')}{cR_o} \qquad \psi' = \frac{\pi\nu_o b(n+n')}{2cR_o}$$

Whereupon equation (78) becomes:

$$= \frac{1}{(\theta_1\theta_2)^2 A_1 A_2 R_o^4}\iint b^2\left(\frac{\sin\psi}{\psi}\right)^2\left(\frac{cR_o}{\pi\nu_o b}\right)^2 d\psi d\psi' \iint a^2\left(\frac{\sin\phi}{\phi}\right)^2\left(\frac{cR_o}{\pi\nu_o a}\right)^2 \cdot \cos\frac{2\phi d}{a}\, d\phi.d\phi'$$

$$= \frac{1}{A_1 A_2}\left[\frac{c^2}{\theta_1\theta_2\pi^2\nu_o^2}\right]^2 \iint \left(\frac{\sin\psi}{\psi}\right)^2 d\psi\, d\psi' \iint \left(\frac{\sin\phi}{\phi}\right)^2 \cos\frac{2\phi d}{a}\, d\phi.d\phi'$$

Since the variables have been changed, it is now necessary to calculate the new limits of integration in the ψ, ψ'- plane.

Now, $-\frac{R_o\theta_2}{2} < n < \frac{R_o\theta_2}{2}$, where $n = \frac{cR_o}{2\pi\nu_o b}(\psi + 2\psi')$,

also, $-\frac{R_o\theta_2}{2} < n' < \frac{R_o\theta_2}{2}$, where $n' = \frac{-cR_o}{2\pi\nu_o b}(\psi - 2\psi')$.

At the upper limit of n : $\psi + 2\psi' = \frac{\pi\nu_o b\theta_2}{c} = \Psi$ (say),

thus $\psi' = \frac{1}{2}(\Psi - \psi)$. (80)

At the lower limit of n : $\psi + 2\psi' = -\Psi$

thus $\psi' = -\frac{1}{2}(\Psi + \psi)$ (81)

At the upper limit of n' : $\psi - 2\psi' = -\Psi$

thus $\psi' = \frac{1}{2}(\Psi + \psi)$ (82)

At the lower limit of n' : $\psi - 2\psi' = \Psi$

thus $\psi' = -\frac{1}{2}(\Psi - \psi)$ (83)

Fig. 2.2 illustrates the area of integration defined by equations (80) to (83) in the ψ, ψ' plane. Summarising, then, we may write each term as:

$$\Delta(\nu_o)\,\Gamma^2(d,\nu_o) = \frac{1}{A_1A_2}\left(\frac{c^2}{\theta_1\theta_2\pi^2\nu_o^2}\right)^2 \int_0^{\Psi}\left(\frac{\sin\psi}{\psi}\right)^2 d\psi$$

$$\cdot \int_{-\frac{1}{2}(\Psi-\psi)}^{\frac{1}{2}(\Psi-\psi)} d\psi' \iint \left(\frac{\sin\phi}{\phi}\right)^2 \cos\frac{2\phi d}{a}\, d\phi\, d\phi',$$

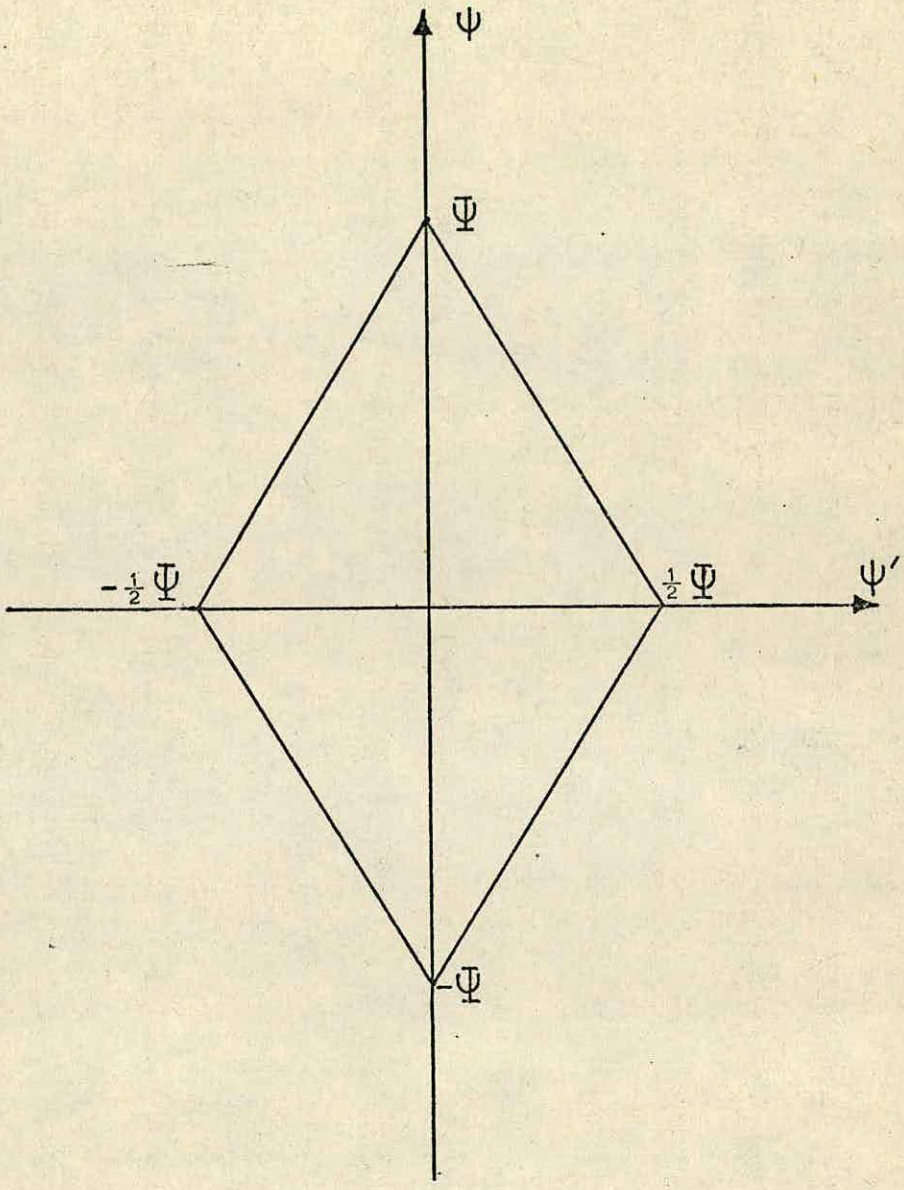

Fig.2.2: Diagram to illustrate the area of integration in the ψ, ψ' plane.

which, on integrating with respect to ', becomes:

$$= \frac{1}{A_1 A_2} \left(\frac{c^2}{\theta_1 \theta_2 \pi^2 \nu_o^2}\right)^2 \int_o^{\Psi} \left(\frac{\sin \psi}{\psi}\right)^2 (\Psi - \psi) d\psi \iint \left(\frac{\sin \phi}{\phi}\right)^2 \cos \frac{2\phi d}{a} \, d\phi \, d\phi'. \tag{84}$$

It is clear, up to this point, that all four terms of $\Delta(\nu_o) \Gamma^2 (d, \nu_o)$ are identical, whether symmetric or antisymmetric. The differences between the terms are evidently about to arise in the integrations over the ϕ, ϕ'-plane. Before carrying out the integrations, the limits have to be recalculated, since the variables have been changed from m and m' to ϕ and ϕ':

Thus in the first symmetric case, we integrate from

$$m = \frac{R_o \theta_3}{2} + R_o \theta_1 \quad \text{to} \quad m = \frac{R_o \theta_3}{2} \tag{a}$$

$$\text{with } m' = \frac{R_o \theta_3}{2} + R_o \theta_1 \quad \text{to} \quad m' = \frac{R_o \theta_3}{2} \tag{b}$$

In the second symmetric case, we integrate from

$$m = -\left(\frac{R_o \theta_3}{2} + R_o \theta_1\right) \text{ to} \quad m = \frac{R_o \theta_3}{2} \tag{c}$$

$$\text{with } m' = -\left(\frac{R_o \theta_3}{2} + R R_o \theta_1\right) \text{ to} \quad m' = \frac{R_o \theta_3}{2} \tag{d}$$

In the first antisymmetric case, we integrate from

$$m = \frac{R_o \theta_3}{2} + R_o \theta_1 \quad \text{to} \quad m = \frac{R_o \theta_3}{2} \tag{e}$$

$$\text{with } m' = \left(\frac{R_o \theta_3}{2} + R_o \theta_1\right) \quad \text{to} \quad m' = -\frac{R_o \theta_3}{2} \tag{f}$$

In the second antisymmetric case, we integrate from

$$M = -\left(\frac{R_o\theta_3}{2} + R_o\theta_1\right) \quad \text{to} \quad m = -\frac{R_o\theta_3}{2} \qquad (g)$$

$$\text{with } m' = \frac{R_o\theta_3}{2} + R_o\theta_1 \quad \text{to} \quad m' = \frac{R_o\theta_3}{2} \qquad (h)$$

Remembering that

$$m = \frac{cR_o}{2\pi\nu_o a}(\phi + 2\phi'), \text{ and } m' = \frac{-cR_o}{2\pi\nu_o a}(\phi - 2\phi').$$

For the limits (a) and (e): $\frac{R_o\theta_3}{2} + R_o\theta_1 = \frac{cR_o}{2\pi\nu_o a}(\phi + 2\phi')$.

then $\phi + 2\phi' = \Phi_3 + 2\Phi$, where $\Phi_3 = \frac{\pi\nu_o a\theta_3}{c}$

and $\Phi = \frac{\pi\nu_o a\theta_1}{c}$

thus $\phi' = \frac{1}{2}(\Phi_3 + 2\Phi - \phi)$ (85)

also, $\frac{R_o\theta_3}{2} = \frac{cR_o}{2\pi\nu_o a}(\phi + 2\phi')$

thus $\phi' = \frac{1}{2}(\Phi_3 - \phi)$ (86)

For limits (b) and (h): $\frac{R_o\theta_3}{2} + R_o\theta_1 = \frac{-cR_o}{2\pi\nu_o a}(\phi - 2\phi')$

thus $\phi' = \frac{1}{2}(\Phi_3 + 2\Phi + \phi)$ (87)

also, $\frac{R_o\theta_3}{2} = \frac{-cR_o}{2\pi\nu_o a}(\phi - 2\phi')$

thus, $\phi' = \frac{1}{2}(\Phi_3 + \phi)$ (88)

For limits (c) and (g): $-\left(\frac{R_o\theta_3}{2} + R_o\theta_1\right) = \frac{cR_o}{2\pi\nu_o a}(\phi + 2\phi')$

thus, $\phi' = -\frac{1}{2}(\Phi_3 + 2\Phi + \phi)$ (89)

also, $-\frac{R_o\theta_3}{2} = \frac{cR_o}{2\pi\nu_o a}(\phi + 2\phi')$

thus, $\phi' = -\frac{1}{2}(\Phi_3 + \phi)$ (90)

For limits (d) and (f): $-(\frac{R_o\Theta_3}{2} + R_o\Theta_1) = \frac{-cR_o}{2\pi\nu_o a}(\phi - 2\phi')$

thus $\phi' = -\frac{1}{2}(\Phi_3 + 2\Phi - \phi)$ (91)

also $-\frac{R_o\Theta_3}{2} = \frac{-cR_o}{2\pi\nu_o a}(\phi - 2\phi')$

thus $\phi' = -\frac{1}{2}(\Phi_3 - \phi)$ (92)

Now, from the integration limits defined above, it will be seen that the integration is now the sumeof eight terms, whose configurations in the ϕ, ϕ' plane may be seen in Fig. 2.3. The lines bounding each area of integration are those defined in equations (85) to (92), with each of the four major areas divided into two parts along a line ϕ = constant. Let the areas be labelled from p to w, as shown.

From inspection of the diagram, and the good behaviour of the integrand, it will be evident that we may double the value of the integral over area p, to include area q, and performaa similar operation for areas r and s.

Let $B = \frac{2}{A_1A_2}\left(\frac{c^2}{\Theta_1\Theta_2\pi^2\nu_o^2}\right)^2 \int_o^{\Psi} \left(\frac{\sin\psi}{\psi}\right)^2 (\Psi - \psi)d\psi$,

then, denoting the limits of integration of ϕ' by the text-numbers of the respective equations, we have:

$$\Delta(\nu_o)\,\Gamma^2(d,\nu_o) = 2B\int_o^{\Phi}\left(\frac{\sin\phi}{\phi}\right)^2 \cos\frac{2\phi d}{a}\,d\phi \int_{88}^{85} d\phi'$$

$$+ 2B\int_o^{\Phi}\left(\frac{\sin\phi}{\phi}\right)^2 \cos\frac{2\phi d}{a}\,d\phi \int_{91}^{90} d\phi'$$

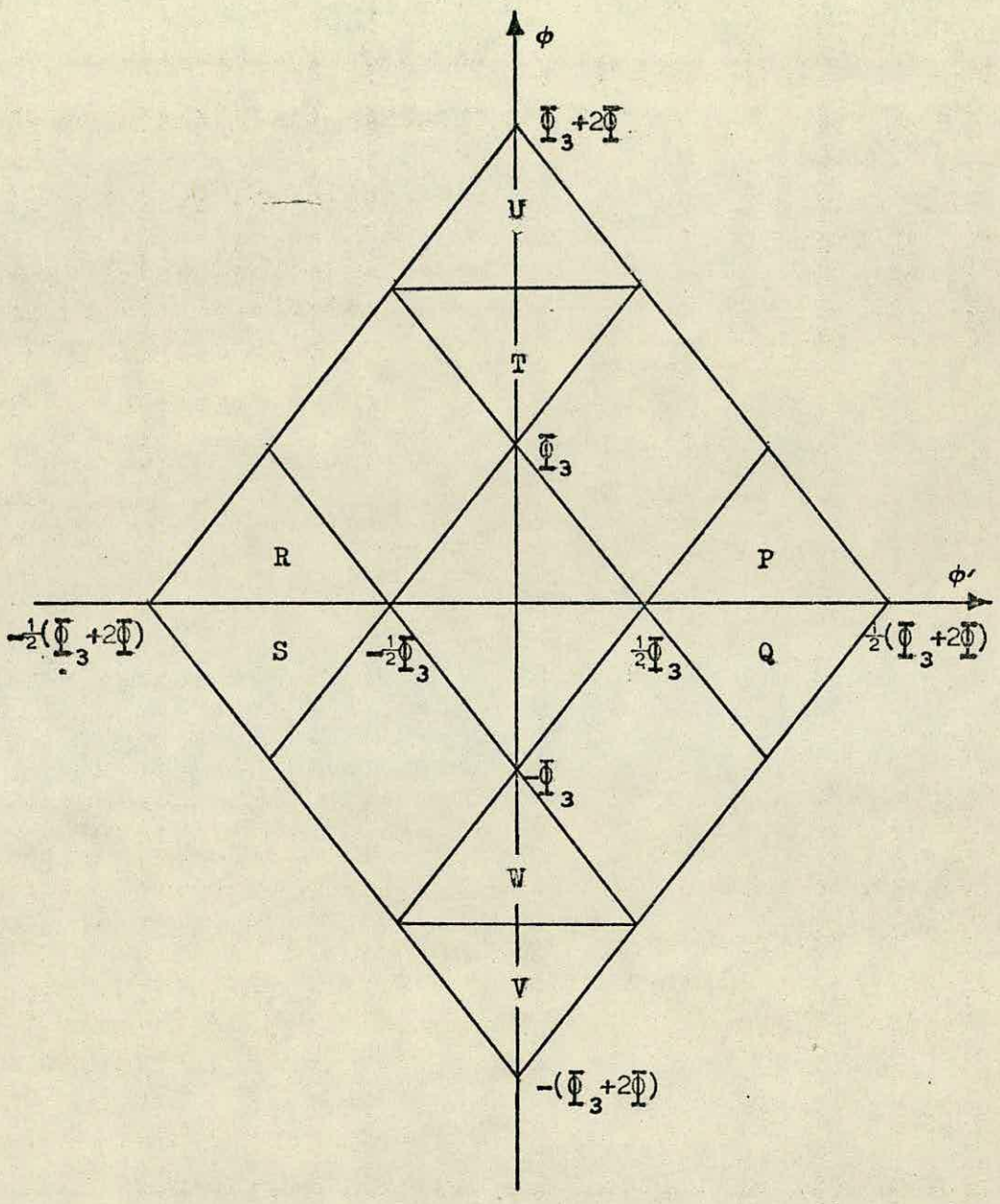

Fig.2.3: Illustrating the areas of integration in the ϕ, ϕ'plane

$$+ B \int_{\Phi_3}^{(\Phi_3+\Phi)} \left(\frac{\sin\phi}{\phi}\right)^2 \cos\frac{2\phi d}{a}\, d\phi \int_{86}^{92} d\phi'$$

$$+ B \int_{(\Phi_3+\Phi)}^{(\Phi_3+2\Phi)} \left(\frac{\sin\phi}{\phi}\right)^2 \cos\frac{2\phi d}{a}\, d\phi \int_{91}^{85} d\phi'$$

$$+ B \int_{-(\Phi_3+2\Phi)}^{-(\Phi_3+\Phi)} \left(\frac{\sin\phi}{\phi}\right)^2 \cos\frac{2\phi d}{a}\, d\phi \int_{89}^{87} d\phi'$$

$$+ B \int_{-(\Phi_3+\Phi)}^{-\Phi_3} \left(\frac{\sin\phi}{\phi}\right)^2 \cos\frac{2\phi d}{a}\, d\phi \int_{88}^{90} d\phi' \qquad (93)$$

Integrating each term of equation (93) separately, and rearranging, we have:

$$\text{Areas } (p+q): \quad 2B \int_0^{\Phi} \left(\frac{\sin\phi}{\phi}\right)^2 \cos\frac{2\phi d}{a}\,(\Phi - \phi)\,d\phi$$

$$\text{Areas } (r+s): \quad 2B \int_0^{\Phi} \left(\frac{\sin\phi}{\phi}\right)^2 \cos\frac{2\phi d}{a}\,(\Phi - \phi)\,d\phi$$

$$\text{Area } t: \quad -B \int_{\Phi_3}^{(\Phi_3+\Phi)} \left(\frac{\sin\phi}{\phi}\right)^2 \cos\frac{2\phi d}{a}\,(\Phi_3 - \phi)\,d\phi$$

$$= B \int_{\Phi_3}^{(\Phi_3+\Phi)} \left(\frac{\sin\phi}{\phi}\right)^2 \cos\frac{2\phi d}{a}\,(\phi' - \Phi_3)\,d\phi$$

$$\text{Area } u: \quad B \int_{(\Phi_3+\Phi)}^{(\Phi_3+2\Phi)} \left(\frac{\sin\phi}{\phi}\right)^2 \cos\frac{2\phi d}{a}\,(\Phi_3 + 2\Phi - \phi)\,d\phi$$

$$\text{Area } v \quad : \quad B \int_{-(\Phi_3+\Phi)}^{-(\Phi_3+\Phi)} \left(\frac{\sin\phi}{\phi}\right)^2 \cos\frac{2\phi d}{a}\,(\Phi_3 + 2\Phi + \phi)\,d\phi$$

$$= B \int_{(\Phi_3+\Phi)}^{(\Phi_3+2\Phi)} \left(\frac{\sin\phi}{\phi}\right)^2 \cos\frac{2\phi d}{a}\,(\Phi_3 + 2\Phi - \phi)\,d\phi$$

$$\text{Area } W \quad : \quad -B \int_{-(\Phi_3+\Phi)}^{(\Phi_3+\Phi)} \left(\frac{\sin\phi}{\phi}\right)^2 \cos\frac{2\phi d}{a}\,(\Phi_3 + \phi)\,d\phi$$

$$= B \int_{\Phi_3}^{(\Phi_3+\Phi)} \left(\frac{\sin\phi}{\phi}\right)^2 \cos\frac{2\phi d}{a}\,(\phi - \Phi_3)\,d\phi \ .$$

Collecting terms, we see that:

$$\Delta(\nu_o)\,\Gamma^2(d, \nu_o) = 4B \int_0^{\Phi} \left(\frac{\sin\phi}{\phi}\right)^2 \cos\frac{2\phi d}{a}\,(\Phi - \phi)\,d\phi$$

$$+ 2B \int_{\Phi_3}^{(\Phi_3+\Phi)} \left(\frac{\sin\phi}{\phi}\right)^2 \cos\frac{2\phi d}{a}\,(\phi - \Phi_3)\,d\phi$$

$$+ 2B \int_{(\Phi_3+\Phi)}^{(\Phi_3+\Phi)} \left(\frac{\sin\phi}{\phi}\right)^2 \cos\frac{2\phi d}{a}\,(\Phi_3 + 2\Phi - \phi)\,d\phi \qquad (94)$$

Now, this expression is still not yet quite true, since each of the four terms (two symmetric, two antisymmetric) contained implicitly in equation (94) in self-normalised, but $\Delta(\nu_o)\,\Gamma^2(d, \nu_o)$ is not. Therefore, to complete the normalisation of the entire equation, each of the four terms must be divided by four. On re-substituting for B,

and normalising the entire expression, the final result becomes:

$$(\nu_o)\,\Gamma^2(d,\nu_o) = \frac{2}{A_1A_2}\left(\frac{c^2}{\theta_1\theta_2\pi^2\nu_o^2}\right)^2\int_o^{\Psi}\left(\frac{\sin\psi}{\psi}\right)^2(\Psi-\psi)\,d\psi$$

$$\cdot\int_o^{\Phi}\left(\frac{\sin\phi}{\phi}\right)^2\cos\frac{2\phi d}{a}\,(\Phi-\phi)\,d\phi$$

$$+\frac{1}{A_1A_2}\left(\frac{c^2}{\theta_1\theta_2\pi^2\nu_o^2}\right)^2\int_o^{\Psi}\left(\frac{\sin\psi}{\psi}\right)^2(\Psi-\psi)\,d\psi$$

$$\cdot\int_{\Phi_3}^{(\Phi_3+\Phi)}\left(\frac{\sin\phi}{\phi}\right)^2\cos\frac{2\phi d}{a}\,(\phi-\Phi_3)\,d\phi$$

$$+\frac{1}{A_1A_2}\left(\frac{c^2}{\theta_1\theta_2\pi^2\nu_o^2}\right)^2\int_o^{\Psi}\left(\frac{\sin\psi}{\psi}\right)^2(\Psi-\psi)\,d\psi$$

$$\cdot\int_{(\Phi_3+\Phi)}^{(\Phi_3+2\Phi)}\left(\frac{\sin\phi}{\phi}\right)^2\cos\frac{2\phi d}{a}\,(\Phi_3+2\Phi-\phi)\,d\phi \qquad (95)$$

This expression was evaluated by means of the Edinburgh Regional Computing Centre's ICL4-75 computer for a number of different values of the detector separation, d. The resulting graph of $\Delta(\nu_o)\Gamma^2(d,\nu_o)$ versus d may be seen in Fig. 4.2 of Chapter 4 and the computer program is the subject of Appendix (a).

The values of $\Delta(\nu_o)\,\Gamma^2(d,\nu_o)$, calculated for different detector spacings, are substituted into equations (70) and (72) to find the predicted values of the Correlation Ration, ρ, and the

Signal to Noise Ratio, S/N. Finally, if it is desired to ascertain the value of $\Delta(\nu_o)$ only, it will be remembered that $\Gamma^2(d, \nu_o) = 1$ when $d = 0$, and therefore $\Delta(\nu_o)\,\Gamma^2(d, \nu_o) = \Delta(\nu_o)$ at zero detector separation.

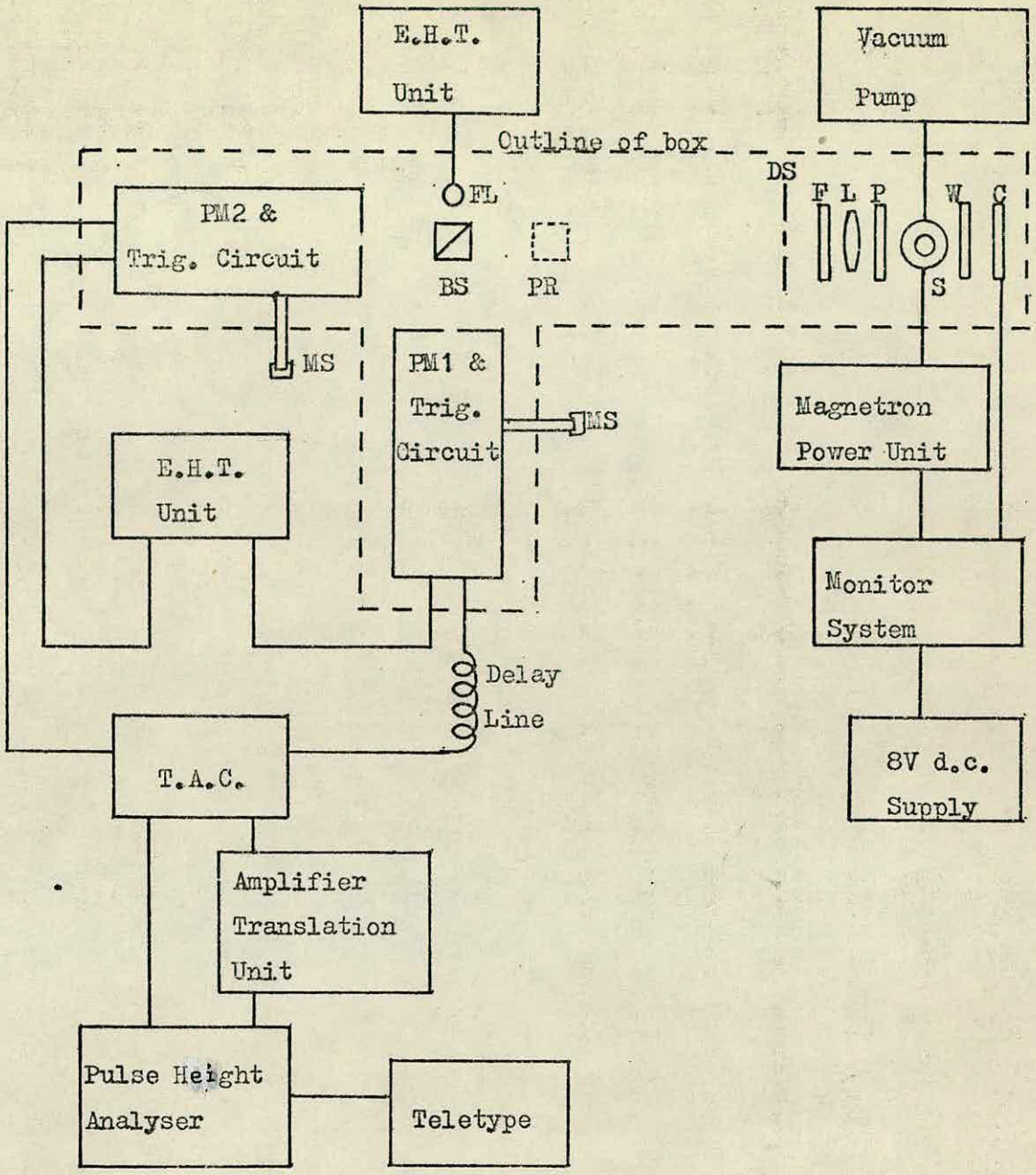

Legend

C Photoseneitive Cell

W Water Cell

S Discharge Tube

L Lens

P Polariser

F Filter

DS Double Slits

BS Beam Splitter

MS Micrometer Screw

T.A.C. Time-to-Amplitude Convertor

FL Flasher

PR Periscope

Fig.3.1: Schematic diagram of apparatus

CHAPTER 3

Description of Apparatus

Section (a) Introduction and the Optical System

A schematic diagram of the complete equipment can be seen in Fig.3.1. The light-proof box, optical system and source system were initially constructed and assembled by Haig. The optical system and box were reconstructed and an improved detection system was assembled by Mrs. W. Sillitto. The entire system was made operational and its performance optimised by the present author.

The primary source, an electrodeless Mercury-198 discharge tube, was imaged by a 2" aperture lens, of 6" focal length, onto the secondary sources, a pair of square apertures, constructed using a preferential etching technique developed by Hill and Rigby[82] (1969). Using this method, one side of a sheet of copper is coated with photoresist. When the photoresist is exposed to ultra-violet radiation through a photoplate image of the desired apertures, the image is reproduced in hardened photoresist. After the liquid photoresist has been washed from its surface, the copper is plated with nickle, leaving bare only those parts, the areas of the apertures, which are protected by the hardened photoresist. With the remaining photoresist removed, the copper is etched away from the apertures, which are then defined by the nickle. This technique allows the production of very small apertures having extremely good edge definition.

A narrow-band, all dielectric interference filter cemented to a broad band filter selected the desired wavelength of the light.

This compound filter, made by Barr and Stroud, fitted inside a brass tube which screwed onto a partition in the light-proof box.

Between the double slits and the beam-splitter, a distance of about 180 cms., were two partitions, both having 3" square apertures to allow passage of the light, but to minimise unwanted reflections and leakages. For the same purpose, the entire inside of the light-proof box, and its contents where possible, were painted black. All the optical components, apart from the filter, were mounted upon bench-saddles astride a triangular-section optical bench, which ran the length of the box.

The Barr and Stroud glass-cube beam-splitter consisted of two right-angled prisms cemented along their common hypotenuse. To compensate for the partially polarising property of the beam-splitter a polarising filter was used, orientated so as to remove the orthogonally polarised components from the two beams emerging from the beam-splitter, since orthogonally polarised beams are uncorrelated.

The detector apertures were mounted on the front faces of a pair of canisters containing the photomultipliers and trigger circuits, and were adjustable by means of tangential screws. The canisters were mounted on carriageways allowing movement, on ball-bearings, in a direction perpendicular to the light beam, and were positioned by micrometer screws. Weights were suspended over pulleys by lines attached to the sides of the canisters, and these held the canisters against the ends of the micrometer screws.

A removable plate, in the roof of the light-proof box, allowed a periscope to be lowered into the beam just before the beam-splitter.

This periscope allowed a visual check to be made on the appearance and alignment of the source slits, or interference pattern, when present, and reversed, it allowed the detector slits to be brought into coincidence.

A mercury-switch, nanosecond flasher, placed at the side of the beam-splitter, was used to locate the prompt channel of the Pulse-Height-Analyser.

Section (b) The Source System

The electrodeless Mercury-198 discharge tube was powered by a Mullard JP2 - 0.2 Magnetron, which had an operating frequency of 2.45 GHz, and was cooled by sucking air, at ambient temperature, through a cooling jacket. A check on the pressure in the cooling tubes was provided by a U-tube manometer, at a point between the discharge tube and the vacuum pump. A waveguide cavity based on the tapered rectangular type of Broida and Chapman[83] (1950), but modified by the addition of a variable-length, quarter wave tuning-stub, was used to excite the source.

The Magnetron was bolted to a large bracket on the other side of which was a heat-sink consisting of a large number of thin brass sheets, spaced out and painted black. The circuits associated with the source system, along with the Magnetron and its power supply, were mounted on two large chassis fitting into a 19" rack. Both chassis had upright front panels into which switches, meters, etc., were inserted. The Magnetron and microwave cavity were connected by RG - 8A/U cable.

The circuit diagram of the Magnetron power-supply is shown in Fig.3.2. The H.T. circuit consisted of a Variac variable mains transformer, controlling the voltage across a 1.6 kV transformer, in series with a full-wave, diode rectifier bridge, the output from which was smoothed by an 8 μF capacitor. The Magnetron required a very hot filament at switch-on and a cooler running filament as soon as the H.T. was applied, which conditions were satisfied by the low-tension circuit consisting of a mains-powered, double-tapped isolating transformer, switched to provide either 4.8 volts or 5.3 volts. This switching was performed by means of a three-way, double-pole wafer switch, the three positions being "off", "5.3 volts" for the initial heating, and "4.8 volts" for when the H.T. power supply was switched on. An Anode Current meter and a voltmeter enabled monitoring of the Magnetron anode current and voltage.

The Magnetron cavity temperature was also monitored. This was achieved by placing a Chromel-Alumel thermocouple, connected to a Spot Galvanometer, in contact with the body of the Magnetron. With the Galvanometer calibrated the cavity temperature could be seen at a glance.

In order to avoid damage to the Magnetron, in the event of a minor fault causing the rated operational conditions of the Magnetron to be exceeded, several safeguards were incorporated into the system. These ensured that the power supply to the Magnetron was cut off whenever the cavity temperature or anode current exceeded pre-set levels.

Overheating was guarded against by placing a Mullard OCP 71 phototransistor in the thermocouple Spot Galvanometer, in such a way

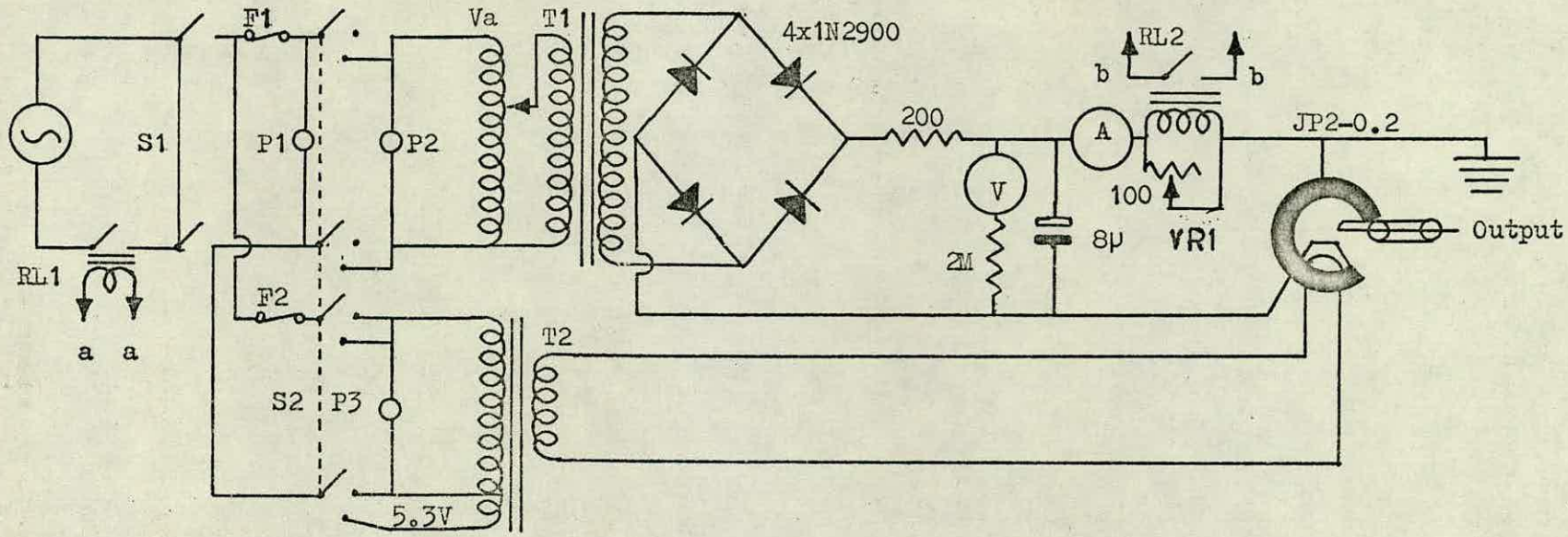

Component List

RL1	Thermal cutout circuit	Va	Variac
RL2	Overload cutout	P1	Master Pilot Lamp
S1	Master Switch	P2	H.T. Pilot Lamp
S2	Selector Switch	P3	Filament Pilot Lamp
F1	3A fuse	V	H.T. Voltmeter
F2	250mA fuse	A	Milliammeter
T1	H.T. Transformer	VR1	Cutout current Potentiometer
T2	Filament Transformer		

Fig.3.2: Circuit diagram of the Magnetron Power Unit.(For connections a and b see Fig.3.3)

as to intercept the light beam just before the Magnetron heat-sink temperature reached the maximum permitted value of 125°C. The phototransistor was arranged to control a relay by means of the circuit shown in Fig. 3.3. When the light beam illuminated the OCP 71, the relay switched off the mains supply to the Magnetron unit, and, in addition, it switched off the 24V d.c. supply to its own circuit. This latter was a precaution ensuring that power was not reapplied to the Magnetron as the temperature fell again. Resetting of this device was by manual operation of a biased switch.

A further protection for the Magnetron unit was the addition of a low-resistance relay to the earthy end of the Magnetron anode circuit. This relay was shunted by a variable resistor, the setting of which determined the anode current at which the relay pulled in and out of the L.T. power supply to the thermal cut-out circuit. The setting of the variable resistance corresponded to the quoted maximum rated current of the Magnetron, 125 mA., and when the relay cut off power to the cut-out circuit, power to the Magnetron unit was locked off until reset with the biased switch.

A relative measure of the discharge intensity was provided by a circuit consisting of an ORP 93 Cadmium Sulphide cell, powered by a 20V d.c. supply by way of a 6.3V Zener diode, with a 20 mA meter registering the resultant current. The ORP 93 was mounted on top of the waveguide and behind the discharge tube. A water-filled glass cell placed between the discharge tube and the Cadmium Sulphide cell protected the latter from ultra-violet radiation.

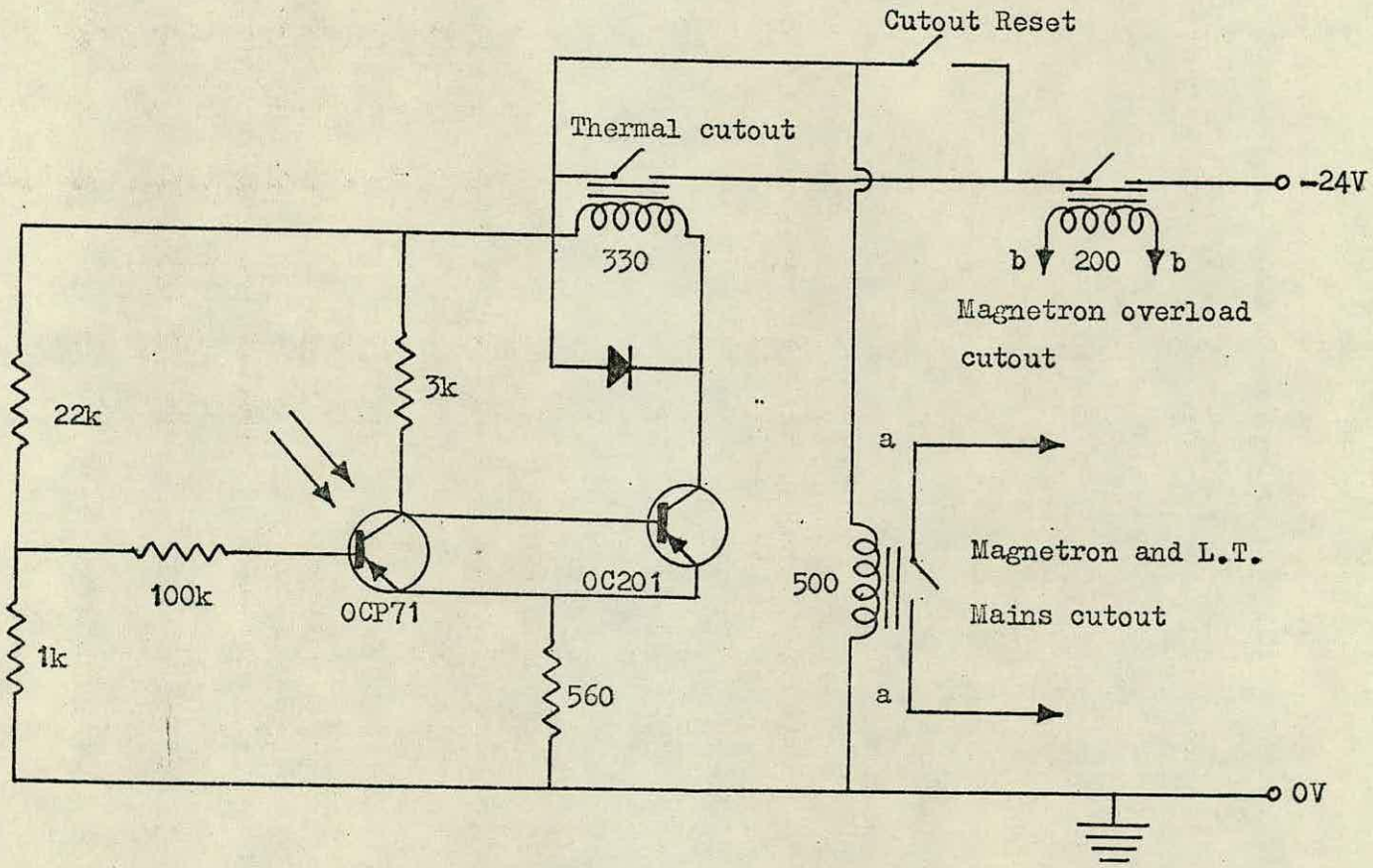

Fig.3.3: Circuit diagram of the phototransistorised Thermal cutout circuit.(For connections a and b see Fig.3.2.)

Section (c) The Detector System

The photomultipliers, along with their dynode resistor chains and the trigger circuits, were contained in the canisters described in the previous section. The 2" diameter photomultiplier tubes, type 9813 KB manufactured by E.M.I., had a venetian blind arrangement of fourteen dynodes. Fig. 3.4 is a diagram of the dynode resistor chain. The cathode was held at a high negative potential and voltage dependent resistors, whose characteristic curve is shown in Fig. 3.5, were used between dynodes. In both canisters, the photomultiplier was supported by a Paxolin ring and by its base, both of which were screwed onto three long rods projecting from the end plate of the canister. The resistor chain was mounted on a Paxolin ring immediately behind the photomultiplier base, and the trigger circuit, mounted upon a 3" square vector board, occupied the remainder of the canister. The high voltages for the photomultipliers were provided by a pair of I.D.L. stabalised H.T. supply units.

The trigger circuits (Fig. 3.6) were designed by Leung and Paul[84] (1968) and built by the staff of the departmental electronics workshop. These circuits were designed to generate fast rise-time, constant-amplitude, rectangular pulses, at the photomultiplier outputs, which would be capable of triggering the Time-to-Amplitude Converter at its rather high level of -2V. The circuit was also designed to be sensitive to small signals but not to the final signal level, the trigger level of the circuit being set by the potentiometer and having a minimum of about 20 mV. Coupling to the anode of the photomultiplier was d.c., and the diode, CR1, provided a.c. coupling and d.c. isolation for test pulses. The amplifier stage matched the trigger circuit

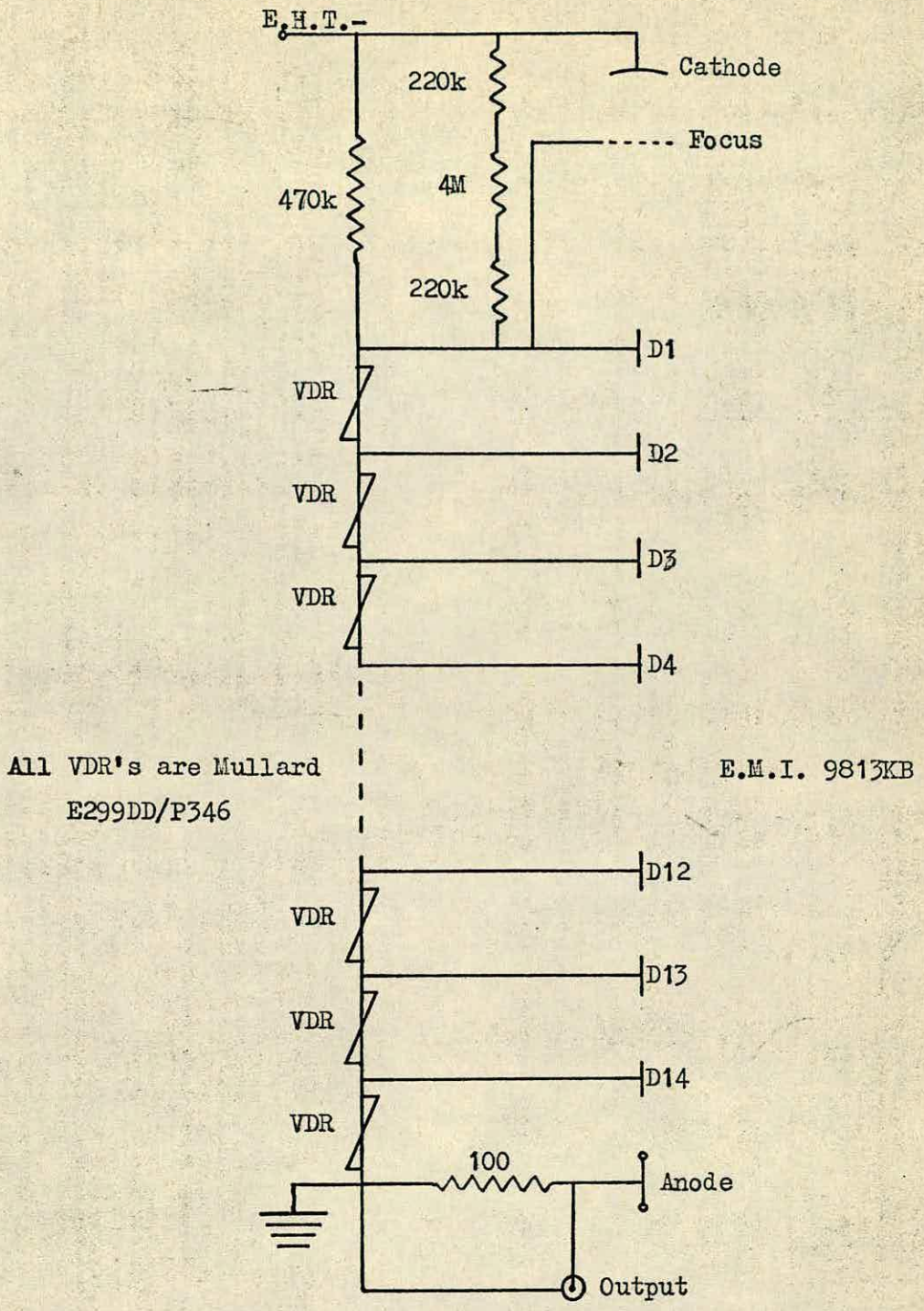

Fig.3.4: Circuit diagram of the dynode resistor chain.

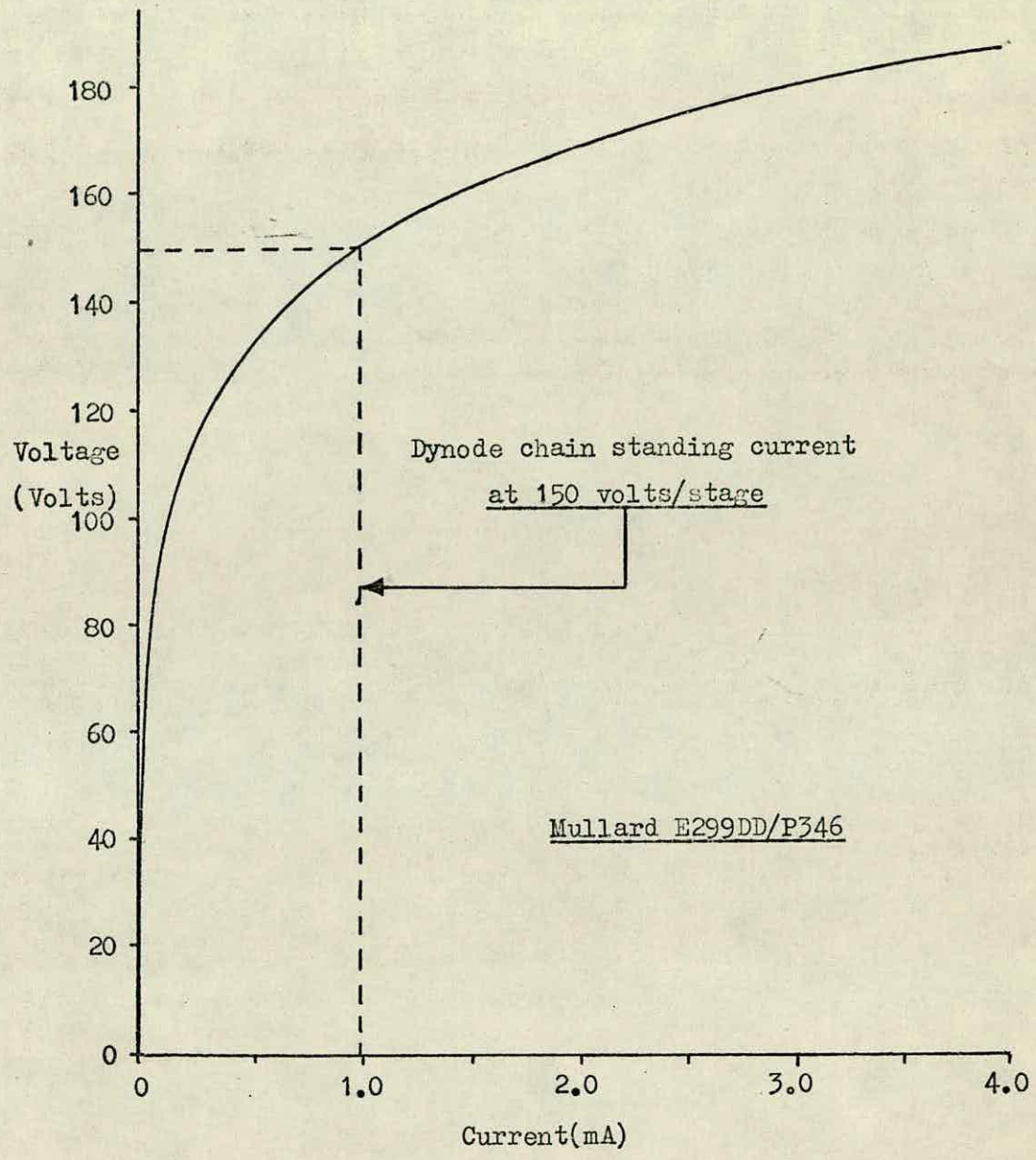

Fig.3.5: Characteristic curve of the Voltage-Dependent Resistors.

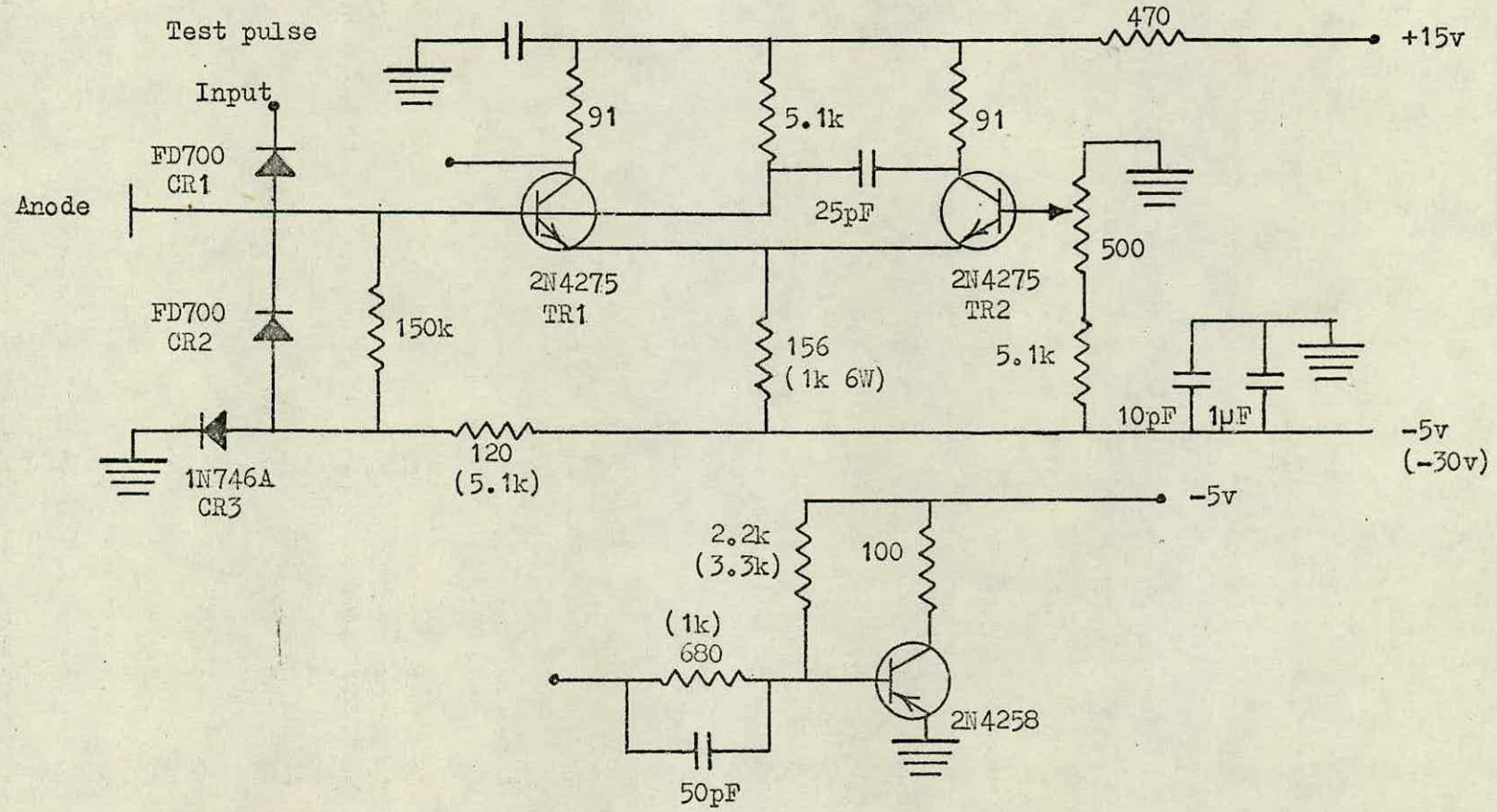

Fig.3.6: Circuit diagram of the trigger circuits. The original values of the components are bracketed where these were different from the final values, and the capacitors at the -5v level were not part of the original circuit.

output to the T.A.C. input. The output pulses, observed on a Tektronix 454 oscilloscope, were extremely clean and square, having an amplitude of -5V and a rise-time of approximately 5 nsecs., most of which was due to the oscilloscope so that, in fact, the rise-time of the pulses was probably only 1 or 2 nsecs.

Initially, the trigger circuits were found to be unstable, a drift in the characteristics of the transistors causing the circuits to oscillate after only a short running time and necessitating rather frequent replacement of transistors. It was therefore thought that some kind of temperature control might be necessary. However, the heat source causing the trouble was found to be the 1K resistor, which was placed in close proximity to the transistors on the vector board, and it was found sufficient to reduce the -30V level to -5V and to replace the 1K resistor by a 156Ω resistor. It was also found necessary to provide a.c. coupling to ground at the -5V level. The initial and final values of the circuit components are both shown in Fig. 3.6. The potentials for the circuit were provided by a Harwell power unit type 2015.

The outputs from the trigger circuits were fed, through As 50 coaxial cables with P.E.T. connectors, into the start and stop inputs of a Harwell Nanosecond Time-to-Amplitude Converter, type 2118. The cable from one trigger circuit to the start input was 90" in length, while the cable from the other trigger circuit to the stop input was 125' in length, representing a delay of 152 n secs. The T.A.C. triggered on negative pulses of -2V amplitude through an impedance of 100Ω . The Time Range, which corresponded to the maximum delay between start and stop input pulses which would produce a pulse at the output, could be

chosen from several values between 50 and 1000 nsecs. The Analogue output pulses from the T.A.C. were approximately rectangular, negative pulses whose amplitude was proportional to the time interval between the start and stop input pulses, with a maximum of -5V, and whose duration could be selected from a number of values in the range 0.2 to 10 μsecs.

The Laben 100-Channel Analyser accepted positive pulses in the range 0.1 to 10V, so it was necessary to translate, as well as amplify, the output pulses from the T.A.C. The T.A.C. output was therefore fed to the Analyser through a Harwell Amplifier Translation unit 2319, which gave an amplification of 2,4,8 or 12 times.

The Analyser had a conversion factor of 50 mV per channel, and the Back-Bias, a ten-turn precision potentiometer permitted the subtraction of a voltage step of between 0.1 and 10V from the input pulses. Besides multichannel operation, the Analyser could also be operated in the Multiscalar mode, which allowed gross counting in each channel for a time preset by an internal clock.

During normal operation, an over-range event at the T.A.C. input produced no pulse at the Analogue output. However, a failure in the T.A.C. caused pulses of arbitrary amplitude to appear, at the Analogue output, whenever an over-range event occurred. It was therefore necessary to gate the Analyser. The T.A.C. provided constant amplitude Output Present pulses, at a second output socket, whenever a within-range event occurred. By feeding these into the coincidence unit of the Analyser, and by demanding coincidence between these and the Direct Input pulses, only within-range events were analysed.

A Teletype connected to the Analogue Output of the Analyser gave a printed or punched paper tape record of the data stored by the Analyser.

CHAPTER 4

Calibration and Theoretical Performance of Equipment

Section (a) Introduction

The theoretical equations determining the quantities to be measured in this experiment have been derived in Chapter 2, but they are now reproduced for ease of reference:

The ratio of correlated coincidence counts to random coincidence counts is given by:

$$\rho = \tfrac{1}{4} \frac{\tau_o}{\tau_r} \Delta(\nu_o)\, \Gamma^2(d, \nu_o)\, f_1 f_2,$$

and the signal-to-noise ratio is given by:

$$S/N = \tfrac{1}{2} N_o \tau_o \Delta(\nu_o)\, \Gamma^2(d, \nu_o)\, f_1 f_2 \left(\frac{T_o}{2\tau_r}\right)^{\frac{1}{2}},$$

where:

τ_o = coherence time of the source

τ_r = resolving time of the detector system

$\Delta(\nu_o)$ = partial coherence factor

$\Gamma^2(d, \nu_o)$ = normalised correlation factor

$f_1 f_2$ = instrumental decorrelation factors

N_o = mean single-channel count rate

T_o = total observing time

The effect to be measured is very small and it can be seen that the signal-to-noise ratio is only proportional to $T_o^{\frac{1}{2}}$. It is apparent therefore that it is important to obtain optimum conditions before running the experiment. This means: obtaining a high beam intensity

and minimising intensity losses in the apparatus; arranging the geometry of the optical system to give optimum values of $\Delta(\nu_o)$; keeping noise, either in the form of reflections and stray light in the optical system, or noise pulses in the electronics, to a minimum; and obtaining a value for $\frac{\tau_o}{\tau_r}$ of near unity. The theory derived in chapter 2 was relevant only in the case of $\frac{\tau_o}{\tau_r} \lesssim 1$, and there is little danger in practice of achieving a value of $\frac{\tau_o}{\tau_r} > 1$ if a thermal light source is used, as in this case.

Section (b) The Source System

From the two equations reproduced in section (a), it can be seen that the source was required to have as high an intensity as possible and as long a coherence length as possible. These two requirements were, of course, related; a higher intensity implying a higher temperature, with a consequent broadening of the spectral line, and hence a decrease in the coherence length.

Two sets of correlation measurements were performed using either of the two most prominent lines, the 4358 Å and the 5461 Å lines, in the visible part of the spectrum of the Mercury Source. An estimate of the coherence lengths of these lines was obtained by observing the path difference, in a Michelson Interferometer, at which the fringes first became invisible. The green fringes were easily observable, but the blue line lies off the peak response of the eye, and so it was impossible to measure the coherence length of the blue line using this method. However, since emission of a quantum of 5461 Å wavelength involved a transition to a metastable state, the green line was

broadened by self-absorption. [Terrien[85], 1960]. Thus, although the Doppler broadened green line would be expected to be narrower than the Doppler broadened blue line, since the width is proportional to the frequency, self-absorption will tend to reduce the difference in width, and the two may be assumed to be comparable.

Using the green line in the Michelson Interferometer, the measured path difference was 27 cms, which gave a value, for the coherence length, of (Cook[86](1962)):

$$c\tau_o \gtrsim 15 \text{ cms},$$

so that the coherence time was:

$$\tau_o \gtrsim 0.5 \text{ nsecs},$$

and this value was assumed for both spectral lines.

The lamp was run at almost its maximum brilliance because, although the coherence length could be increased by about 0.5 cms by running the magnetron at less than its maximum permissible ratings, the corresponding decrease in intensity out-weighed the increase in coherence length.

In order to maximise the intensity, it was important that the waveguide should be carefully tuned, and that the lamp should be carefully positioned in the waveguide. Power loss in the cable connecting the magnetron to the waveguide was kept to a minimum by shortening the cable as much as possible. Also, the lamp was kept scrupulously clean.

Section (c) The Optical System

The optical system consisted of a pair of identical square source apertures, a pair of identical rectangular detector apertures, a lens focusing the light from the lamp onto the source apertures, a beam-splitter, and a polariser.

The Partial Coherence Factor, $\Delta(\nu_o)$, was a function of the size and shape of the apertures, and it is desirable to maximise this factor, which, since $\Delta(\nu_o)$ is normalised, means achieving a value as close to unity as possible. An increase in the value of $\Delta(\nu_o)$ is obtained by decreasing the size of the apertures. However, this also reduced the photoelectron counting rate, and so it is the product, $N_o \Delta(\nu_o)$, which has to be maximised.

In addition, the width of the source apertures must be less than their separation, the width of the detector slits must be less than half the width of the central maximum of the correlation pattern, and also, the width of the detector slits must not be so large as to allow an appreciable spread in the photoelectron transit-times. The dimensions of the apertures are shown in Fig. 4.1.

The predicted shape and separation of the maxima of the correlation pattern were checked experimentally by placing a single slit between the lamp and the double slits and observing the visible interference pattern of the source apertures. The separation of the maxima, for both the green and the blue spectral lines, lay within less than 2% of the predicted value, and the shape of the maxima corresponded fairly well with the predicted shapes, but depended largely on the width of the primary slit.

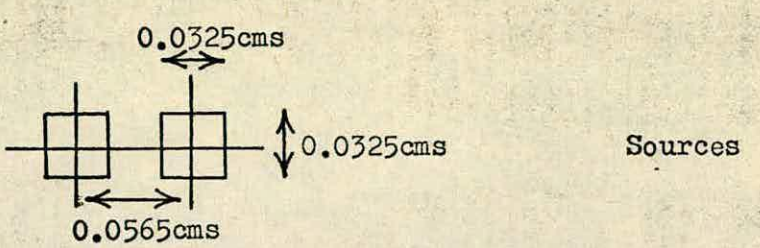

Source to Detector distance (R_0) = 180cms

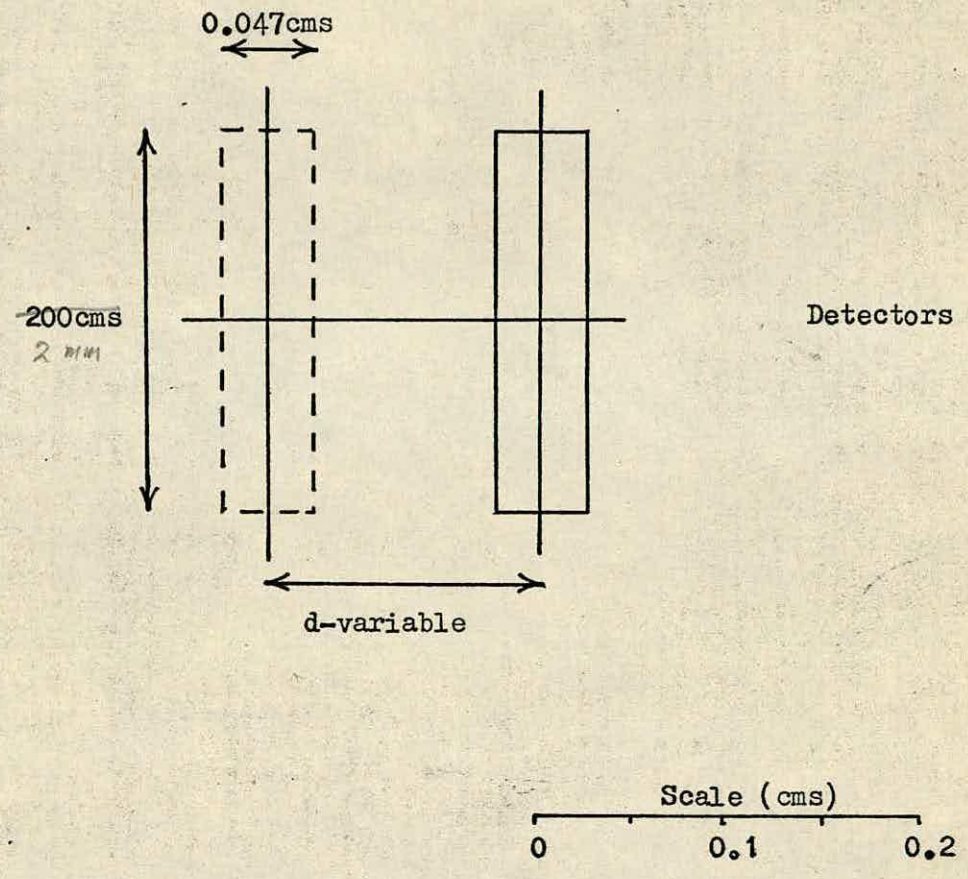

Fig.4.1: Scale diagram of the Source and Detector Apertures.

The Normalised Correlation Factor, $\Gamma^2(d, \nu_o)$, was a function of the detector separation, d, being unity for d = o, falling to a minimum as d increased, and rising to a secondary maximum for values of d which were different for the two wavelengths.

The aim of the experiment was to measure the correlation ratio at several detector separations using the 5461Å line, and then to repeat the measurements at the same separations, but using the 4358 Å line. The graphs of the variations of $\Delta(\nu_o)\,\Gamma^2(d, \nu_o)$ with d are shown in Fig. 4.2.

Since the orthogonally polarised components of the light beam were not correlated, a sheet of Polaroid polarising material was used to select a single component. The factof f_1 in equation (70) represented the loss of correlation due to the polarising effect of the beam splitter, so, with the insertion of the polariser, f_1 became equal to unity. The reduction, in the counting rate, due to the polariser and the beam splitter was 60%.

The final loss of intensity in the optical system was due to the photomultipliers. According to the spectral response curve of the 9813 KB photomultipliers, as published by the manufacturers, the quantum efficiency at 4358 Å is $\sim$ 22%, and at 5461 Å is $\sim$ 10%. In fact, the count-rate for the green line was slightly higher than for the blue line, which suggests that the green line was the stronger, in terms of photon flux.

It was important that the two source apertures should be radiating independently. If there was any coherence between the sources, it would appear as a variation of the intensity across the plane scanned

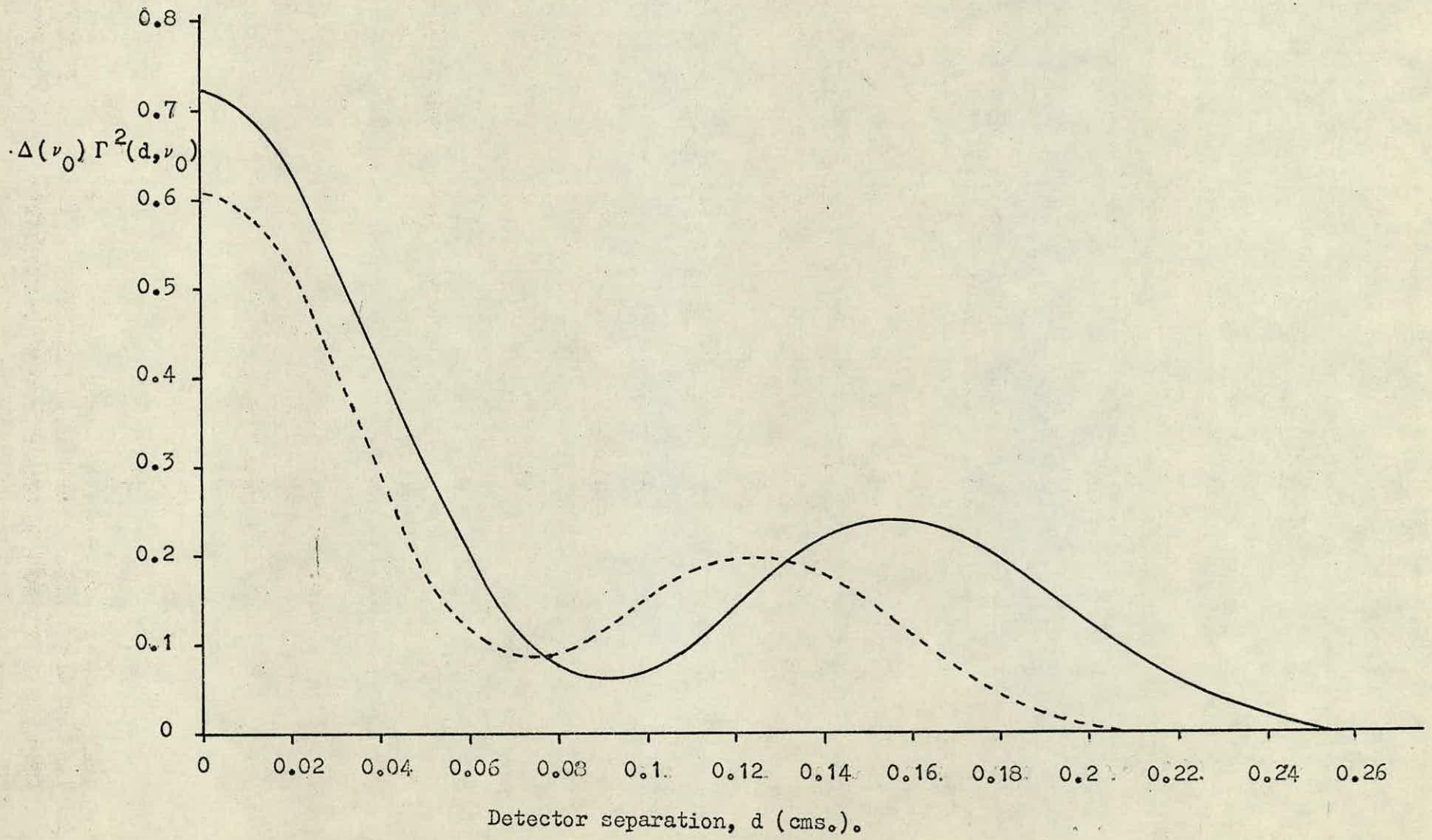

Fig.4.2: Graph of $\Delta(\nu_0)\,\Gamma^2(d,\nu_0)$ versus detector separation, d.

by the detectors. Originally the focusing had been arranged to produce a fairly large image of the lamp on the source slits, and, with this arrangement, an interference pattern was detectable. However, with the focusing adjusted so that the image of the lamp was only slightly broader than the width of the pair of apertures, the pattern disappeared.

Section (d) The Detector System

The characteristics of the photomultipliers, quoted by the manufacturers, were as follows:

9813 KB serial no:	5565	5566
Photocathode Sensitivity:	68 μ A/L	72 μ A/L
Gain:	10^8 at 2160V	10^8 at 2390V
Dark Current:	3 nA at 2160V	13 nA at 2390V

The E.H.T. supply to number 5565 was maintained at 2.3 KV, and to number 5566 at 2.6 KV. These were close to the maximum operating voltages but were adjusted so that the single channel counting rates in both photomultipliers were equal. At these voltages the dark current counting-rates were 9% and 3%, for number 5566 and number 5565 respectively, of the illuminated counting-rates.

The factor f_2, in the equations for ρ and S/N, represents the loss of correlation due to noise in the detector system, and was measured by recording coincidences between dark current pulses in one

photomultiplier and light pulses in the other. Defining f_2 as:

$$f_2 = \frac{\bar{R}_{12} - \bar{R}_{10}}{\bar{R}_{12}},$$

where $\bar{R}_{12}$ = mean random illuminated coincidences count rate,

and $\bar{R}_{10}$ = mean random illuminated coincidence count rate with one photomultiplier covered,

and averaging the results for each photomultiplier in turn, the value obtained was:

$$f_2 = 0.87$$

A range of 250 nsecs was selected on the Time-to-Amplitude Converter, and an amplification of 4x on the Amplifier, so that, remembering that the maximum pulse height of the T.A.C. output was -5V, and that the Analyser had a conversion factor of 50 mV/chan., the expected time-scale on the Analyser was 4 chans./2.5 nsecs. This was checked experimentally by dividing the output from one photomultiplier, and using it to trigger the T.A.C. start input through a short cable, and the stop input through a longer delay cable. This cable had a time delay of 1 nsec per 9.25", so by varying the delay length the Analyser could be calibrated. Again, the time-scale of the Analyser was found to be 4 chans./2.5 nsecs.

The prompt-coincidence channel of the Analyser was located by observing the coincidence peak which was obtained when the photomultipliers were illuminated by the nanosecond light pulses from the Mercury Switch flasher. Fig. 4.3 is a photograph of the coincidence peak of the flasher, obtained in a counting time of about 15 mins.

The fall-time, as well as the rise-time, of the output pulses

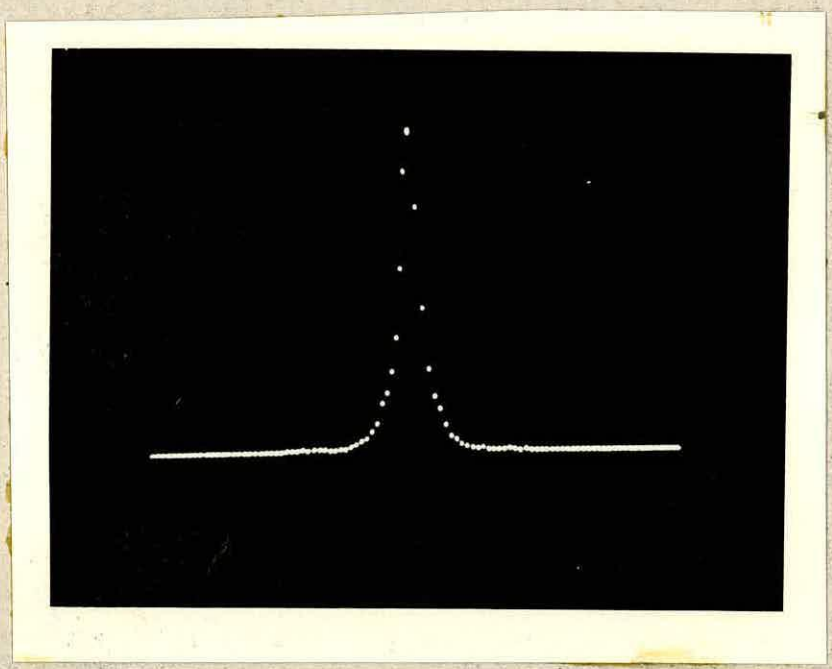

Fig. 4.3: Photograph of the coincidence peak of the flasher.

(4 chans./2.5 nsecs.)

from the trigger circuits, was fast, their duration was determined by the lengths of the photomultiplier pulses, and the circuits appeared to be ready for retriggering as soon as they had set. It seemed, therefore, that there was little or no dead-time associated with the trigger circuits. The trigger levels of the circuits were set so as to bias against dark current pulses, but to trigger on light pulses.

According to the manufacturers, the T.A.C. had a dead-time of:

$$T_a + T_b + T_c + 2.4\ \mu \text{ secs}$$

where T_a = interval between start and stop input pulses

T_b = time range selected

T_c = 1.1 μ secs for a time range of 250 nsecs.

The maximum dead-time was thus 4 μ secs, which can have had little effect on an average single channel counting-rate of $< 10^4$ counts/sec.

The resolving time of the detector system was taken as half the width, at half-height, of the correlated coincidence peak. The full width at half-height was three channels, giving a resolving time of:

$$2\tau_r = 1.88 \text{ nsecs}$$

That most of this was due to the transit-time spread of electrons in the photomultipliers was apparent from the fact that, when both the start and stop inputs of the T.A.C. were triggered by the divided pulses from one photomultiplier, the counting was almost entirely confined to only one channel.

With all the variables in the equation for ρ known, we can now calculate the theoretical values for ρ, and this will be done in the next chapter.

CHAPTER 5

Experimental Readings and Results

Section (a) Measuring Procedure

Measurements of the delayed coincidence spectra were performed using first the green and then the blue Mercury lines, using the same procedure in both cases. The delayed coincidence spectrum was recorded at various detector separations, d, between 0 and 0.17 cms, and at each separation the total counting time was six days. The distribution of counts recorded by the Analyser was printed out, by the Teletype, after a continuous counting time of three days, so that each total of six days was the result of two three-day counting periods. Occasionally a three-day period was broken into two shorter counting periods, but the total was still three days.

The three-day coincidence spectra were obtained as follows: while one photomultiplier was kept stationary the other photomultiplier was moved, by means of the micrometer screw, to each position from d = 0 cms out to d = 0.17 cms and then back from d = 0.17 cms to the superposed position. By counting at each position twice in this way, the effects of back-lash, on the position of the photomultiplier, were averaged.

Using the green line, the delayed coincidence spectra were recorded at d = 0, 0.025, 0.0425, 0.085, 0.11, 0.15, and 0.17 cms, and using the blue line, at d = 0, 0.025, 0.0425, 0.075, 0.11, 0.13, 0.15 and 0.17 cms. Thus a total of thirty delayed coincidence spectra were recorded during a total time of ninety days. The data were analysed by computer.

Section (b) Readings and Results

Figs. 5.1 and 5.2 show photographs of three of the coincidence spectra obtained, using the green line, at photomultiplier separations of 0, 0.085 and 0.17 cms. The correlated coincidences form a peak of width $2\tau_r$, or 3 channels, centred on the prompt channel of the Analyser, so the number of correlated coincidences was obtained by summing the counts, N_p, registered in these three channels, and subtracting the random background. The random coincidences were those, registered in channels outside the central peak, having a delay greater than τ_r. The random coincidence channels were grouped in threes, and the mean number of random coincidences, $\bar{N}_r$, was obtained by finding the average number of counts per group of three channels. The ratio of correlated to random coincidences was then given by:

$$\rho = \frac{N_p - \bar{N}_r}{\bar{N}_r} \qquad (a)$$

It was expected that the random coincidences would be distributed according to Poissonian statistics, and this was verified by calculating the expectation values of the second and third factorial moments of each distribution.

Rewriting the correlation ratio as:

$$\rho = \frac{N_p}{\bar{N}_r} - 1$$

the error in is given by:

$$\left(\frac{\delta\rho}{\rho+1}\right)^2 = \left(\frac{\delta N_p}{N_p}\right)^2 + \left(\frac{\delta \bar{N}_r}{\bar{N}_r}\right)^2$$

(a)

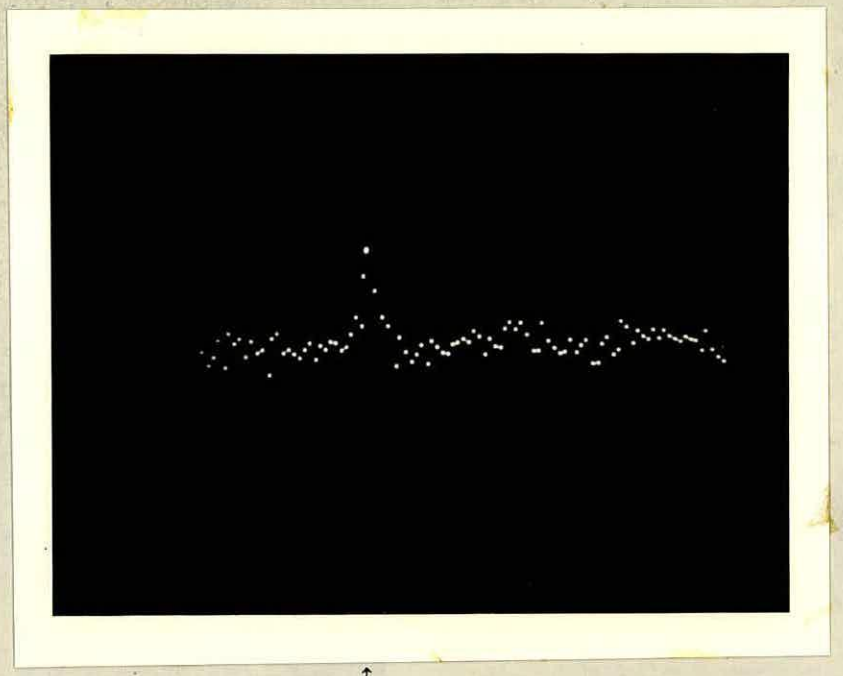

↑

Prompt channel.

(b)

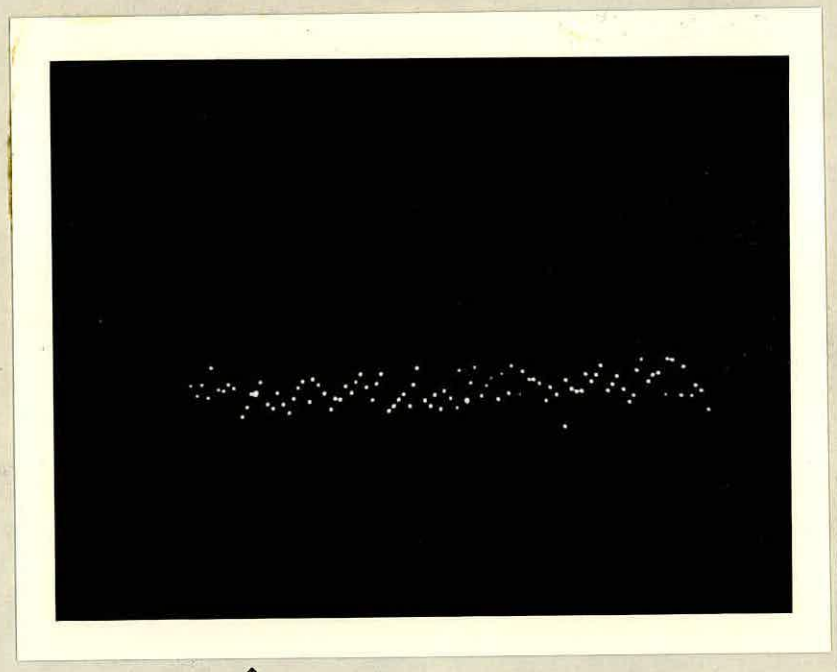

↑

Fig. 5.1: Photographs of coincidence peaks, obtained using the 5461 Å line, at photomultiplier separations of (a) d=0.00 cms. and (b) d=0.085 cms.

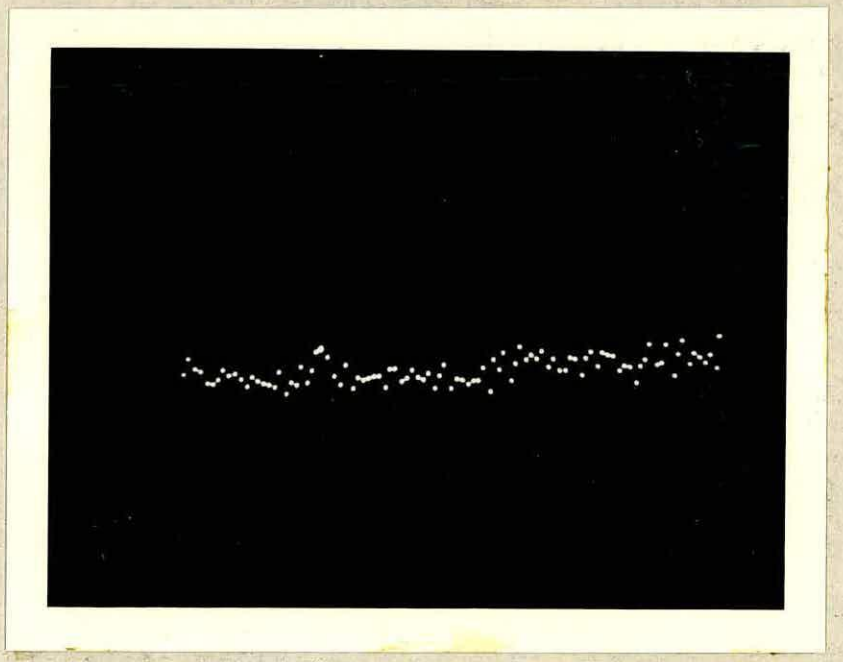

Prompt channel

Fig. 5.2: Photograph of the coincidence peak obtained, using the 5461 Å line, at a photomultiplier separation of d=0.17 cms.

It is well known that the variance of a Poisson distribution is equal to the square-root of the mean, thus:

$$\delta N_r = N_r^{\frac{1}{2}}$$

Now, $\bar{N}_r$ was the mean of C groups of 3 channels, therefore:

$$\delta \bar{N}_r = \frac{\delta N_r}{C}$$

Although the distribution of correlated coincidences was not expected to be Poissonian, the correlation effect was very small, so, for the purpose of calculating the error, it was assumed that:

$$\delta N_p = N_p^{\frac{1}{2}}$$

Thus the error in the correlation ratio is given by:

$$\left(\frac{\delta \rho}{\rho+1}\right)^2 = \left(\frac{1}{N_p^{\frac{1}{2}}}\right)^2 + \left(\frac{1}{C\bar{N}_r^{\frac{1}{2}}}\right)^2 \qquad (b)$$

When the Analyser was gated, the number of channels used was limited. Also, when calculating the mean random coincidence count-rate, the three correlated coincidence channels, plus one group of three channels on either side of the peak, were not used. The number of groups of three channels used to calculate $\bar{N}_r$ was then 20, and with this value for C, the error in the mean number of random coincidence counts was negligible compared with the error in the number of correlated coincidence counts.

The values obtained for $\bar{N}_r$ and ρ, at each detector separation, are presented in Table I for the 5461Å line, and in Table II for the 4358Å line. In both tables the results are divided into two sections, one section showing those obtained when the photomultiplier was being

Table I

Numbers of mean random coincidence counts and ratios of correlated to random coincidences for the 5461 Å line

Photomultiplier Separation, d (cms)	Out from centre			In towards centre			Mean
	$\bar{N}_r$	ρ	$\bar{\rho}$	$\bar{N}_r$	ρ	$\bar{\rho}$	$\bar{\rho}$
0	14831	0.083	0.083	9902	0.096	0.085	0.084 ± 0.004
0	14501	0.083	± 0.006	17708	0.079	± 0.006	
0.025	25803	0.062 ± 0.006		21436	0.076 ± 0.007		0.068 ± 0.005
0.0425	10557	0.058	0.061	20860	0.03 ± 0.007		0.045 ± 0.005
0.0425	9964	0.064	± 0.007				
0.085	18707	0.003 ± 0.008		28005	0.004 ± 0.006		0.004 ± 0.005
0.11	7063	0.014	0.011	7770	0.015	0.016	0.013 ± 0.004
0.11	24916	0.01	± 0.006	16253	0.017	± 0.007	
0.15	23393	0.029 ± 0.007		24664	0.024 ± 0.006		0.026 ± 0.005
0.17	22589	0.024 ± 0.007		26497	0.022 ± 0.006		0.023 ± 0.005

Table II

Numbers of mean random coincidence counts and rates of correlated to random coincidences for the 4358Å line.

Photomultiplier Separation, d(cms)	Out from centre			In towards centre			Mean
	$\bar{N}_r$	ρ	$\bar{\rho}$	$\bar{N}_r$	ρ	$\bar{\rho}$	$\bar{\rho}$
0	10406	0.076	0.067	12546	0.08	0.071	0.068 ± 0.005
0	10353	0.055	± 0.007	9166	0.059	± 0.007	
0.025	19294	0.053 ± 0.007		24340	0.041 ± 0.007		0.046 ± 0.005
0.0425	22395	0.028 ± 0.007		31576	0.026 ± 0.006		0.027 ± 0.004
0.075	34790	0.008 ± 0.006		30748	0.01 ± 0.006		0.009 ± 0.004
0.11	20735	0.017 ± 0.007		31812	0.02 ± 0.006		0.019 ± 0.004
0.13	35008	0.021 ± 0.005		13242	0.029	0.024	0.023 ± 0.004
0.13				27237	0.022	± 0.005	
0.15	12160	0.023	0.025	22186	0.012 ± 0.007		0.02 ± 0.004
0.15	17422	0.027	± 0.006				
0.17	25853	0.008 ± 0.006		29539	0.011 ± 0.006		0.01 ± 0.004

moved outwards from the superposed position, the other showing those obtained when the photomultiplier was being moved in towards the superposed position. Where a coincidence spectrum was obtained during two counting periods, the results for each period are shown along with the weighted mean, where the weight is according to $\bar{N}_r$. The final column shows the value for the correlation ratio obtained by taking the weighted mean of the values in both sections.

Comparing the results in the two sections, it would appear that back-lash did affect the values of ρ, these tending to be higher when the photomultiplier was moved from a point of higher correlation to a point of lower correlation, and vice-versa. However, the effect of back-lash should be largely eliminated in the combined results.

The results for both spectral lines are presented graphically in Fig. 5.3, where the error bars represent the statistical errors calculated according to equation (b). The curves represent the theoretical variation of the correlation ratio, calculated using equation (70), at intervals of 0.01 cms.

It can be seen that the experimental values are in good agreement with the theoretical values, most lying close to the theoretical curves, and all, except for one point, at $d = 0.025$ cms, on the blue line, lying on the theoretical curves within the limits of statistical accuracy. In addition, it can be seen that the two spectral lines are well resolved.

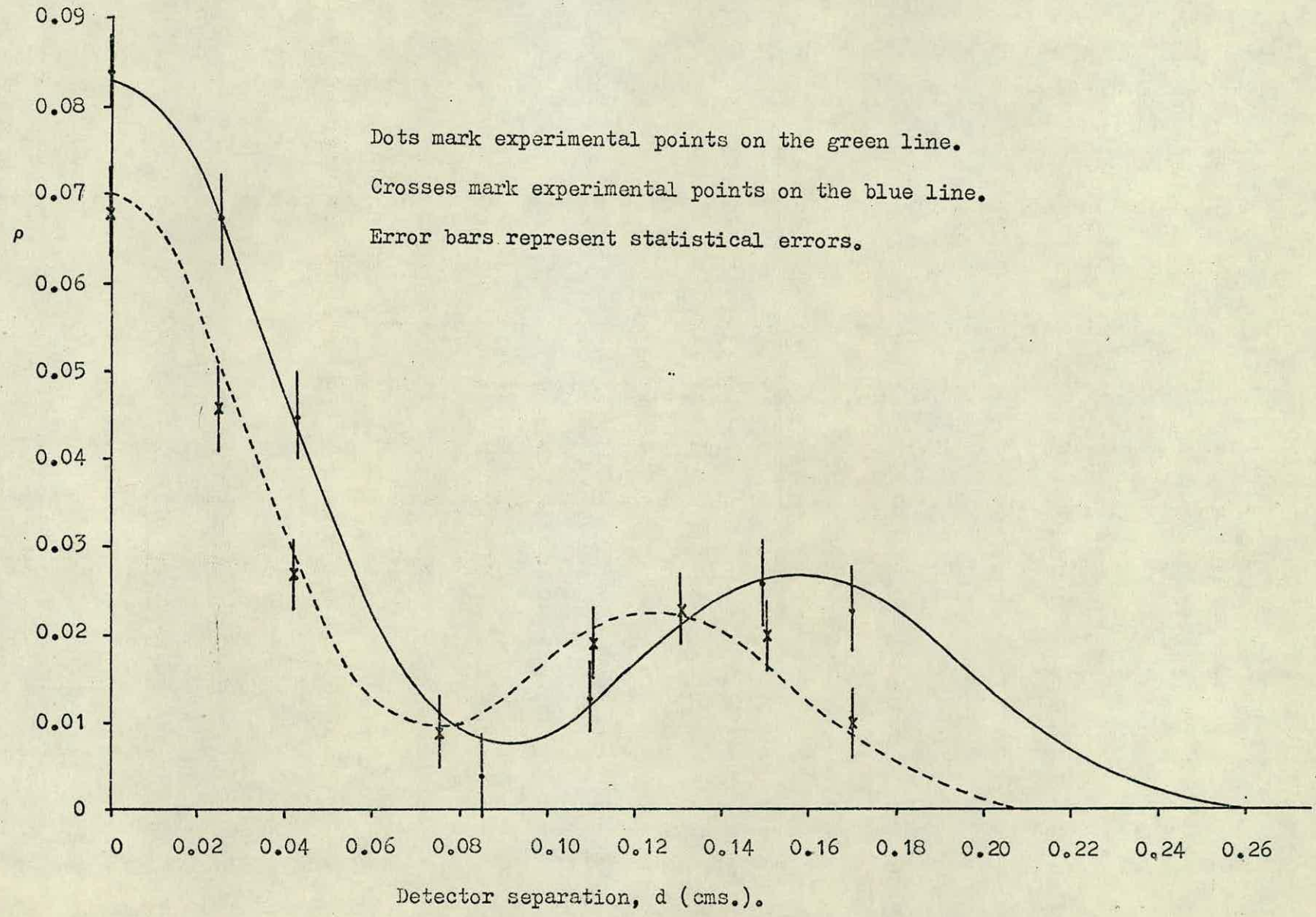

Fig.5.3: Graph of the ratio of correlated to random coincidences versus detector separation, d.

Section (c) Conclusion and Discussion of Results

In chapter 5 the experimental values of the correlation ratio were compared, graphically, with the theoretical curves. However, these "theoretical" curves were also subject to experimental error, and an attempt was made to estimate a value for these errors.

The error in $\Delta(\nu_o)\,\Gamma^2(d, \nu_o)$ was estimated by substituting the maximum and minimum values of the various geometrical measurements into the integration limits in the computer program. It was thus found that the error in $\Delta(\nu_o)\,\Gamma^2(d, \nu_o)$ varied from $\sim 2\%$ at the central maxima, to a negligible value at the minima, and to $\sim 10\%$ at the secondary maxima.

The resolving time of the detector system was calculated as the average half-width of 12 coincidence peaks, each with a signal-to-noise ratio > 5, giving:

$$\tau_r = 0.94 \pm 0.03 \text{ nsecs}$$

The measurement of the path difference in the Michelson Interferometer could not have been in error by more than 0.5 cms, giving:

$$\tau_o = 0.5 \pm 0.005 \text{ nsecs},$$

and the decorrelation factor was estimated to be accurate to within $\sim 2\%$.

Combining these errors;using the formula:

$$\left(\frac{\delta\rho}{\rho}\right)^2 = \left(\frac{\delta\tau_r}{\tau_r}\right)^2 + \left(\frac{\delta\tau_o}{\tau_o}\right)^2 + \left(\frac{\delta(\Delta\Gamma^2)}{\Delta\Gamma^2}\right)^2 + \left(\frac{\delta f_2}{f_2}\right)^2 \qquad (c)$$

gave values for $\delta\rho$ ranging from 0.003 at the central maxima down to

negligibly small values at the minima, and up to 0.003 at the second maximum on the green line, and 0.002 at the second maximum on the blue line. These values can be compared with the statistical errors in Tables I and II of chapter 5. Although these two sets of errors, statistical and observational, are not of the same nature, for expediency these are combined according to the formula:

$$\left(\frac{\delta \rho}{\rho}\right)^2 = \left(\frac{\delta \rho_1}{\rho_1}\right)^2 + \left(\frac{\delta \rho_2}{\rho_2}\right)^2$$

Fig. 5.4 presents again the theoretical curves and experimental points, but now the error bars represent the combined statistical and observational errors.

The largest single contribution to the total error in ρ is the statistical error. Of course, a longer counting time would have reduced the variance of the delayed coincidence spectrum, however, it will be remembered that the signal-to-noise ratio varied as the square-root of the counting time, so doubling the counting time would have reduced the statistical error by only 25%. There was therefore, little to be gained by extending the counting time.

The magnitudes of the experimental errors approached those of the statistical errors at the tops of the central and secondary maxima, where small errors in the measurements of the geometry of the optical system could produce relatively large errors in the values of $\Delta(\nu_o)\,\Gamma^2(d, \nu_o)$. The error in the resolving time accounted for most of the remainder of the experimental error, the errors in the coherence time and the decorrelation factor being relatively small.

It can be seen from Fig. 5.4 that, with the combined errors, the

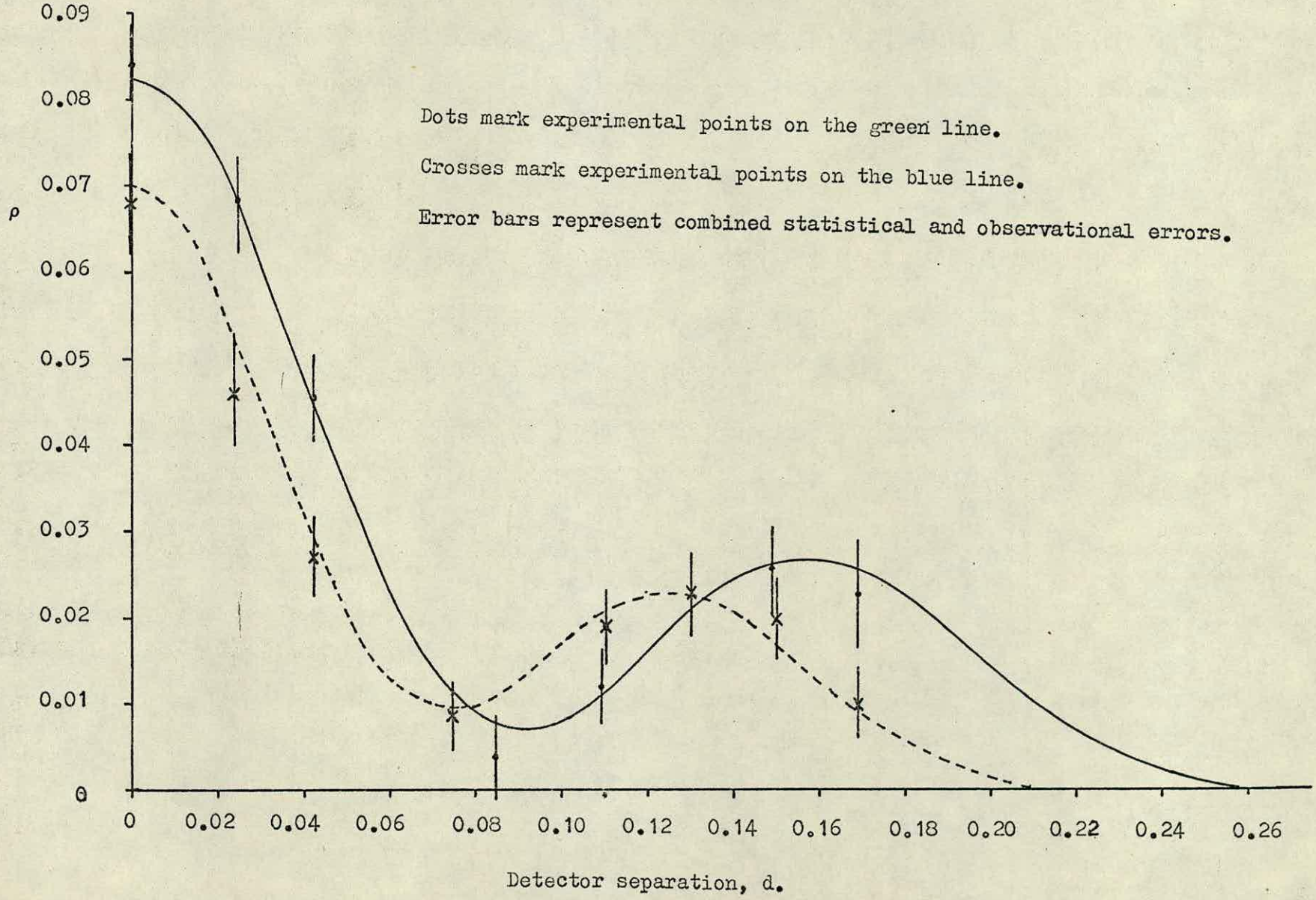

Fig.5.4: Graph of the ratio of correlated to random coincidences versus detector separation, d.

two lines are still well resolved, and the very small reduction in the errors that might have been gained by extending the counting time, or by using more sophisticated methods to estimate the values of the experimental quantities involved in the calculations of the theoretical values of the correlations, would not have been worth the time spent.

It can be concluded, then, that second-order coherence effects have been observed, and that these are in good quantitative agreement with the theory. Also, the results can be interpreted as demonstrating interference between two independent thermal light sources.

ACKNOWLEDGEMENTS

I would like to extend my grateful thanks to my supervisor, Mr. R.M. Sillitto, and to Mrs. W. Sillitto for their ready assistance and advice throughout the course of this work. I would also like to thank Professor Cochran for placing the facilities of the Physics Department at my disposal.

My thanks are also due to the staff of the Electronics Workshop for their prompt and efficient repair of my electronic equipment.

Finally, I wish to thank the Science Research Council for the award of a Postgraduate Studentship.

APPENDIX (a) The Computer Program for Calculating $\Delta(\nu_o)\,\Gamma^2(d, \nu_o)$

```
begin
real PHI,PHI 3,PHI 4,PHI 5,PSI,sum,K,y,tin,ter,hin,her,bin,ber,r,w
integer k,i
real fn spec twiss(real x)
real fn spec hanbury(real x)
real fn spec brown(real x)
routine spec aut(real fn f,real a,b,e,real name int,erint,integer k)
read(PHI);read(PHI 3);read(PHI 4);read(PHI 5);read(PSI);read(K);read(w)
!limits of integration and common factor


newlines(4);spaces(20);print string('spacing');spaces(8)
print string('correlation');newline


aut(twiss,0,PSI,0.00001,tin,ter,10); vertical integration


cycle i=0,1,60
      r=i/w*100
      k=intpt ((r+20)*0.5)
y=PHI; aut(hanbury,0,PHI,0.00001,hin,her,k);!areas p,q,and r,s
y=PHI 3;aut(brown,PHI 3,PHI 4,0.00001,bin,ber,k);!areas t,w
sum=2*hin+bin:                          !areas p,q,r,s,t,w
y=PHI 5;aut(hanbury,PHI 4,PHI 5,0.00001,hin,her,k);!areas u,v
sum=sum+hin;                            !total area
!common factors including twiss integral are put in in print instructions
newline;spaces(20);print((w*r),1,4);spaces(10);print((K*tin*sum)/4,1,5)
repeat


real fn twiss(real x);        !depends on vertical displacements
if x<0.025 then -> 1
result =((sin(x))/x)**2*(PSI-x)
1: result=PSI-x
end


real fn hanbury(real x);      !areas p,q,r,s or u,v according to limits
if x<0.025 then -> 1
result=((sin(x))/x)**2*(y-x)*(cos(r*x)
1: result=(x-y)*cos(r*x)
end
```

```
real fn brown(real x);          !areas t,w
if x<0.025 then -> 1
result=((sin(x))/x)**2*(x-y)*cos(r*x)
1: result=(x-y)*cos(r*x)
end


routine aut(real fn f,real a,b,e,real name int,erint,integer k)
real h,sa,sb,fa,fb,fc,fd,fe,maxh
real fn spec f(real x)
integer n
int=0; fa=f(a); n=0
maxh=(b-a)/k
h=maxh;-> 2
1: h=b-a
2: fc=f(a+0.5h); fe=f(a+h)
3: fb=f(a+0.25h); fd=f(a+0.75h)
sa=(fa+4fc+fe)*h/6; sb=(fa+4fb+2fc+4fd+fe)*h/12
-> 4 if mod(sa-sb)<e
h=½h;fe=fc;fc=fb;-> 3
4: int=int+sb;n=n+1
-> 5 if a+h=b;a=a+h
h=2h unless 2h>maxh;fa=fe
-> 1 if a+h>b;-> 2
5: erint=e*n/15
end


end of program
```

References

(1) Verdet, E., Am. Sci. l'Ecole Normale Superieure, 2 (1865) 291.

(2) Fizeau, H., C.R. Acad. Sci. Paris, 66 (1968) 934.

(3) Michelson, A.A., Phil. Mag., 30 (1890) 1.

(4) Michelson, A.A., Phil. Mag., 31 (1891) 338.

(5) van Cittert, P.H., Physica, 1 (1934) 201.

(6) Zernike, F., Physica, 5 (1938) 785.

(7) Hopkins, H.H., Proc. Roy. Soc. (London), 208 (1951) 263.

(8) Hopkins, H.H., Proc. Roy. Soc. (London), 217 (1953) 408.

(9) Hopkins, H.H., Proc. Roy. Soc. (London, B70 (1957) 1002.

(10) Hopkins, H.H., J. Opt. Soc. Am., 47 (1957) 508.

(11) Wolf, E., Proc. Roy. Soc. (London), A225 (1954) 96.

(12) Wolf, E., Proc. Roy. Soc. (London), A230 (1955) 246.

(13) Wolf, E., Nuovo Cim., 13 (1959) 1165.

(14) Blanc-Lapierre, A., and Dumontet, P., Rev. Opt., 34 (1955) 1.

(15) Dumontet, P., Publ. Sci. Univ. Alger. Ser. B, 2 (1956) 203.

(16) Pancharatnam, S., Proc. Indian Acad. Sci., A44 (1956) 247.

(17) Pancharatnam, S., Proc. Indian Acad. Sci., A45 (1957) 1.

(18) Pancharatnam, S., Proc. Indian Acad. Sci., 57 (1963) 218.

(19) Hanbury-Brown, R., and Twiss, R.Q., Nature, 177 (1956) 27.

(20) Hanbury-Brown, R., and Twiss, R.Q., Proc.Roy.Soc. (London), A243 (1957) 291.

(21) Twiss, R.Q., Little, A.G. and Hanbury-Brown, R., Nature, 180 (1957) 324.

(22) Rebka, G.A. and Pound, R.V., Nature, 180 (1957) 1035.

(23) Brannen, E., Ferguson, H.I.S. and Wehlau, W., Can. J. Phys., 36 (1958) 871.

(24) Twiss, R.Q. and Little, A.G., Austr. J. Phys., 12 (1959) 77.

(25) Wolf, E., "Proc. of the Symp. on Optical Masers", (John Wiley,1963).

(26) Mandel, L., "Quantum Electronics", eds. N. Bloembergen and P. Grivet, (Columbia University Press, 1964).

(27) Wolf, E., "Quantum Electronics", eds. N. Bloembergen and P. Grivet (Columbia University Press, 1964).

(28) Glauber, R.J., Phys. Rev. Letts., 10 (1963) 84.

(29) Glauber, R.J., Phys. Rev., 130 (1963) 2529.

(30) Glauber, R.J., Phys. Rev., 131 (1963) 2766.

(31) Titulaer, U.M. and Glauber, R.J., Phys. Rev. B, 140 (1965) 676.

(32) Wolf, E., Proc. Phys. Soc., 71 (1958) 257.

(33) Mandel, L., Proc. Phys. Soc., 74 (1959) 233.

(34) Mandel, L., J. Opt. Soc. Am., 51 (1961) 797.

(35) Mandel, L., J. Opt. Soc. Am., 52 (1962) 1407.

(36) Kastler, A., "Quantum Electronics", eds. N. Bloembergen and P. Grivet, (Columbia University Press, 1964).

(37) Mandel, L., Sudarshan, E.C.G. and Wolf, E., Proc. Phys. Soc., 84 (1964) 435.

(38) Glauber, R.J., "Quantum Optics and Electronics", eds. C. de Witt, A. Blandin, and C. Cohen-Tannoudji (Gordon and Breach, 1965).

(39) Sillitto, R.M., Nature, 179 (1957) 1127.

(40) Hanbury-Brown, R. and Twiss, R.Q., Proc. Roy. Soc. (London, A242 (1957) 300.

(41) Sudarshan, E.C.G., Phys. Rev. Letts., 10 (1963) 277.

(42) Sudarshan, E.C.G., "Proc. of the Symp. on Optical Masers", (John Wiley, 1963).

(43) Mandel, L. and Wolf, E., Phys. Rev., 149 (1966) 1033.

(44) Mandel, L., "Electromagnetic Theory and Antennas, part 2", ed. E.C. Jordan, (MacMillan, 1963).

(45) Morgan, B.L. and Mandel, L., Phys. Rev. Letts., 16 (1966) 1012.

(46) Arecchi, F.T., Gatti, E. and Sona, A., Phys. Letts., 20 (1966) 27.

(47) Scarl, D.B., Phys. Rev. Letts., 17 (1966) 663.

(48) Scarl, D.B., Phys. Rev., 175 (1968) 1661.

(49) Wolf, E. and Mehta, C.L., Phys. Rev. Letts., 13 (1964) 705.

(50) Mandel, L., Proc. Phys. Soc., 72 (1958) 1037.

(51) Mandel, L., Proc. Phys. Soc., 74 (1959) 233.

(52) Mandel, L., "Progress in Optics" vol.II, ed. E. Wolf (North-Holland, 1963).

(53) Kelly, P.L. and Kleiner, W.H., Phys. Rev. A, 136 (1964) 316.

(54) Bedard, G., Phys. Rev., 151 (1966) 1038.

(55) Srinivasan, S.K. and Sukuvanam, S., J. Phys. A, 5 (1972) 682.

(56) Jakeman, E. and Pike, E.R., J. Phys. a, 1 (1968) 128.

(57) Saleh, B.E.A., J. Appl. Phys., 46 (1975) 943.

(58) Forrester, A.T., Gudmundsen, R.A. and Johnson, P.O., Phys. Rev., 99 (1955) 1691.

(59) Javan, A., Ballik, E.A. and Bond, W.L., J. Opt. Soc. Am., 52 (1962) 96.

(60) Lipsett, M.S. and Mandel, L., Nature, 199 (1963) 553.

(61) Radloff, W., Phys. Letts. A, 27 (1968) 366.

(62) Radloff, W., Ann. Physik, 26 (1971) 178.

(63) Magyar, G. and Mandel, L., Nature, 198 (1963) 255.

(64) Haig, N.D. and Sillitto, R.M., Phys. Letts. A, 28 (1968) 463.

(65) Haig, N.D., Ph.D. Thesis, University of Edinburgh (1968).

(66) Pfleegor, R.L. and Mandel, L., Phys. Letts. A, 24 (1967) 1084.

(67) Pfleegor, R.L. and Mandel, L., Phys. Rev., 159 (1967) 1084.

(68) Pfleegor, R.L. and Mandel, L., J. Opt. Soc. Am., 58 (1968) 946.

(69) Sillitto, R.M. and Wykes, C., Phys. Letts. A, 39 (1972) 333.

(70) Chandra, N. and Prakash, H., Phys. Rev. A, 1 (1970) 1696.

(71) Weber, H.P., I.E.E.E. J. Quantum Electronics, 7 (1971) 189.

(72) Simaan, H.D. and Loudon, R., J. Phys. A, 8 (1975) 539.

(73) Every, I.M., J. Phys. A, 8 (1975) L69.

(74) Clauser, J.F., Phys. Rev. D, 9 (1974) 1397.

(75) Stoler, D., Phys. Rev. Letts., 33 (1974) 1397.

(76) Carmichael, H.J. and Walls, D.F., J. Phys. B, 9 (1976) 1199.

(77) Kimble, J.H., Dagenais, M. and Mandel, L., Phys. Rev. Letts., 39 (1977) 691.

(78) Jakeman, E., Pike, E.R., Pusey, P.N. and Vaughan, J.M., J. Phys. A, 10 (1977) L257.

(79) Born, M. and Wolf, E., "Principles of Optics", (Pergamon Press, 1965).

(80) Parrent, G.B., J. Opt. Soc. Am., 49 (1959) 787.

(81) Parrent, G.B., Optica Acta, 6 (1959) 285.

(82) Hill, A.E. and Rigby, P.A., J. Phys. E, 2 (1969) 1084.

(83) Broida, H.P. and Chapman, M.W., Anal. Chem., 30 (1950) 2049.

(84) Leung, C.Y. and Paul, D.A.L., I.E.E.E. Trans. Nucl. Sci., 15 (1968) 531.

(85) Terrien, J., "National Physical Laboratory Symp. no.11; Interferometry", (H.M.S.O., 1960).

(86) Cook, A.H., Optica Acta, 9 (1962) 55.